HEPATOCELLULAR CARCINOMAS, EXHIBITING INTRATUMOR FIBROSIS, EXPRESS CANCER-SPECIFIC EXTRACELLULAR MATRIX REMODELING AND WNT/TGFB SIGNATURES, ASSOCIATED WITH POOR OUTCOME

Romain Desert [1], Wei Chen [1], Xiaodong Ge [1], Roselyne Viel [2], Hui Han [1], Dipti Athavale [1], Sukanta Das [1], Zhuolun Song [1], Daniel Lantvit [1], Luis Cano [3], Alexandra Naba [4, 5], Orlando Musso [3] and Natalia Nieto [1, 4, 5]

[1] Department of Pathology, University of Illinois at Chicago, 840 S. Wood Ave, Suite 130 CSN, Chicago, IL 60612, USA

[2] Univ Rennes, CNRS, INSERM, UMS Biosit, Core Facility H2P2, 35000 Rennes, France.

[3] INSERM, Univ Rennes, UMR 1241, Nutrition, Métabolismes et Cancer (NuMeCan), 2 Rue Henri le Guilloux, 35000 Rennes, France.

[3] Department of Physiology and Biophysics, University of Illinois at Chicago, 835 S Wolcott Ave, Room E202, MC 901, Chicago, IL 60612, USA

[4] University of Illinois Cancer Center, 818 S. Wolcott Ave, Chicago, IL 60612, USA

[5] Department of Medicine, Division of Gastroenterology and Hepatology, University of Illinois at Chicago, 840 S. Wood St, Suite 1020N, MC 787, Chicago, IL 60612, USA

Corresponding Author: Natalia Nieto, Department of Pathology, University of Illinois at Chicago, 840 S. Wood St, Suite 130 CSN, MC 847, Chicago, IL 60612, USA. Fax: +1 (312) 996-1217. Phone: +1 (312) 355-0774. E-mail: nnieto@uic.edu

Keywords: diethylnitrosamine, liver cancer, tumor classification, tumor microenvironment

Abbreviations: CCl_4, carbon tetrachloride; DE, differentially expressed; DEN, diethylnitrosamine; ECM, extracellular matrix; FC, fold-change; GEO, gene expression omnibus; GSEA, gene set enrichment analysis; HCC, hepatocellular carcinoma; IPA, ingenuity pathway analysis; LF, liver fibrosis; MO, mineral oil; MS, mass spectrometry; NES, normalized enrichment score; NT, non-tumor; PCA, principal component analysis; SR/FG, Sirius red/Fast green; TCGA, the cancer genome atlas; TMT, tandem mass tags.

SUPPLEMENTARY MATERIAL AND METHODS

Induction of HCC and LF in mice. C57BL/6J WT mice were purchased from the Jackson Laboratory (Bar Harbor, ME). Diethylnitrosamine (DEN) was used to induce HCC because it causes tumors, with histologic and genetic features like human HCC (1). Mice were injected i.p. with 20 mg/kg of DEN (Sigma, St. Louis, MO), at 14 days of age, and sacrificed 1 year later (2). To induce LF, mice were injected i.p. twice a week with 0.5 ml/kg of CCl_4 (Sigma), or equal volume of mineral oil (MO), for 1 mo. Livers were collected and fixed in 10% neutral-buffered formalin, and processed into paraffin sections for H&E staining, to pathologically characterize HCC. All animals received humane care according to the criteria outlined in the 'Guide for the Care and Use of Laboratory Animals', prepared by the National Academy of Sciences, and published by the National Institutes of Health.

Tandem mass tags (TMT) mass spectrometry (MS). Decellularized samples were grouped into five batches, and labeled with TMT10plex isobaric label reagent (ThermoFisher, Waltham, MA). Twenty ug of peptides were re-suspended in 50 µl of 50 mM triethylammonium bicarbonate buffer, and ~160 µg of TMT reagents in 20.5 µl of anhydrous acetonitrile were added. After 2 h of incubation at room temperature, the reaction was quenched with 4 µl of hydroxylamine, for 15 min. A combined equal amount of each batch was dried and desalted with a primed HLB 96-well plate for high-pH reverse phase fractionation. Labeled peptides in each batch were separated into 70 fractions with a XBridge BEH C18 Column, 130Å, 3.5 µm, 4.6 x 250 mm (Waters Corporation, Milford, MA). Every tenth fraction was concatenated together, and 10 concatenated fractions were dried, and resuspended in 72 µl of 5% acetonitrile and 2% formic acid buffer. Four µl of staggered high-pH reverse phase fractions, were analyzed using Q Exactive HF MS coupled with an UltiMate 3000 RSLC nanosystem with a nanospray frex ion source (ThermoFisher Scientific). Samples were loaded into a PepMap C18 cartridge (0.3 x 5 mm, 5 µm particle) trap column, and then a 75 µm x 150 mm PepMap C18 analytical column (ThermoFisher Scientific), and separated

at a flow rate of 300 nl/min. Solvent A was 0.1% formic acid in water, and solvent B 0.1% formic acid and 80% acetonitrile in water. The solvent gradient for liquid chromatography was 5% B 0-3 min, 5-30% B 85 min, 30-95% B 90 min, wash with 95% 94.8 min, followed by 5% B 95 min, and equilibration 105 min. Full MS scans were acquired in the Q-Exactive mass spectrometer over 350-1400 m/z range, with a resolution of 120,000 (at 200 m/z) from 5 to 95 min. The AGC target value was 3.00E+06 for the full scan. The 15 most intense peaks with charge states 2, 3, 4, and 5, were fragmented in the HCD collision cell, with a normalized collision energy of 32%. These peaks were excluded for the 30 s within a mass window of 1.2 m/z. A tandem mass spectrum was acquired in the mass analyzer, with a resolution of 60,000. The AGC target value was 1.00E+05. The ion selection threshold was 2.45E+3 counts, and the maximum allowed ion injection time was 50 min for full scans, and 120 min for fragment ion scans.

Database search and statistical analysis. All MS/MS samples were analyzed using Mascot 2.6.2 (Matrix Science, London, UK). Search was carried out against the Uniprot-human_20210601 database (20,386 entries), assuming the digestion enzyme strict trypsin. Mascot was searched with a fragment ion mass tolerance of 0.30 Da, and a parent ion tolerance of 15 ppm. O-110 of pyrrolysine, u+49 of selenocysteine, and carbamidomethyl of cysteine were specified in Mascot, as fixed modifications. Gln→pyro-Glu of the N-terminus, deamidated of asparagine, and glutamine, oxidation of methionine, lysine (Hyl), and proline (Hyp), and TMT-6plex of lysine, and the N-terminus, were specified in Mascot as variable modifications. Scaffold 5.0.0 (Proteome Software Inc., Portland, OR), was used to validate the MS/MS based peptide, and protein identifications. Peptide identifications were accepted if established at greater than 92% probability, to achieve an FDR<1% by the percolator posterior error probability calculation (3). Protein identifications were accepted if established at greater than 5% probability, to achieve an FDR<1%, and contained at least 2 identified peptides. Protein probabilities were assigned by Protein Prophet (4). Proteins that contained similar peptides and could not be differentiated based

on MS/MS analysis alone, were grouped to satisfy the principles of parsimony. Proteins sharing significant peptide evidence were grouped into clusters.

For statistical analysis, using pooled samples as a reference reporter ion for each batch, each sample was entered into four categories in the Quantitation module of the Scaffold Q+. Only two categories were compared in the quantitative testing tab, using Mann Whitney test. Significant difference in protein abundance was considered for FDR<0.05. Gene sets with significant difference between groups (high-grade HCC, n=10; low-grade HCC, n=10; high-grade NT, n=10; low-grade NT, n=10), were then analyzed using IPA (Qiagen, Hilden, GE), to obtain canonical pathway and upstream regulator analyses.

Statistical analysis of publicly available datasets

General methodology. **Supplementary Table 1** contains the publicly available transcriptome profiling datasets used for in silico analysis. Raw data were extracted from the Gene Expression Omnibus (GEO) or the cBioPortal. Patients from the Cancer Genome Atlas (TCGA) cohort were selected for survival analysis using a previously described pipeline (5). Microarray data were normalized, and the log2 intensity expression values for each probe set were calculated by robust multi-array average. Outliers were removed, and batch effects corrected using COMBAT [*R* package sva (6)] in one of the datasets (GSE14520). Probes detected over background, in at least one sample, were quantile normalized (*R* package preprocessCore). To analyze gene expression among HCC subclasses in the 1,133 HCCs metadata set, we used a protocol described previously (5). The list of matrisome genes was downloaded from the MatrisomeDB (7-9). They were identified by proteomics analysis of the ECM fraction, in healthy tissues (colon, lung, liver) and diseased tissues (melanoma, fibrotic lung, primary colon carcinoma). Core matrisome comprises ECM glycoproteins, collagens, and proteoglycans. Matrisome-associated proteins include ECM-affiliated proteins, ECM regulators, and secreted factors. Hierarchical

clustering was performed with the Ward's method using 1-Pearson correlation as a distance metric. Gene selection leading to new HCC subclasses was performed, using a stepwise method further detailed. Gene set enrichment analysis (GSEA) (10) was performed on a comprehensive gene set collection available at the Molecular Signatures Database (Broad Institute, Boston, MA), and using (www.gsea-msigdb.org). Survival analyses were performed using the Log Rank test, and Kaplan-Meier curves. Statistical analyses were performed with *R* 4.1.1.

Expression pattern and annotation. The list of matrisome genes (n=1,027) was downloaded from the matrisome project website (http://matrisomeproject.mit.edu). mRNA expression was analyzed in the six datasets listed in **Supplementary Table 1**. Differential expression (DE) analysis was performed between NT liver and HCC, in four datasets, and between our previously published four robust HCC subclasses, in a 1,133 HCCs metadata set (5). *P* values were calculated by Student's *t*-test. For T vs NT analysis, DE analysis was done separately, in the four datasets, and the result was included only if it was the same in all the available datasets. Otherwise, it was considered non-significant. This yielded three results per gene: T vs NT, PP vs ECM, and PP vs STEM, each of which being upregulated, downregulated, or non-significant. This produced 25 different patterns of expression **(Fig. 4** and **Supplementary Table 2)**. Based on the analysis of their shape, every pattern was manually annotated into eight categories: *NT liver fibrosis*, *common fibrosis*, *ECM*, *fibrous nest*, *stable*, *STEM*, *tumor*, and *undetermined*.

Gene selection identifies new HCC subclasses. We analyzed the expression of matrisome genes available in the 1,133 HCCs metadata set. Of note, only 578 genes commonly available, and expressed over the background in the nine datasets forming the metadata set, were available. Correlation networks among these genes were performed using Pearson's coefficient. Different thresholds were used (R^2=0.35, R^2=0.4, R^2=0.45), resulting in different networks, visualized using Cytoscape (11). They highlighted a network enriched in genes of the *fibrous nest* pattern, and a

second network enriched in genes of the *NT-liver fibrosis* pattern **(Fig. 5A)**. To identify genes representative of *fibrous nest*, *NT-liver fibrosis*, and *biliary/stem HCCs*, we used the following method:

1) For every analysis, we fixed a threshold of Pearson's coefficient, representing strong correlation: 0.6 for *fibrous nest* and *liver fibrosis*, and 0.5 for *biliary/stem*. This threshold was called *t*, onward.
2) Analyzing the correlation network with the lowest threshold (R^2=0.35), we extracted the list of genes within the *fibrous nest* and *liver fibrosis* networks.
3) For the extraction of *robust fibrous* nest and *NT-liver fibrosis* genes, we first selected the matrisome genes with Pearson's correlation >*t*, with at least one gene within the corresponding network (*fibrous nest* or *liver fibrosis*).
4) These two lists of genes were then refined using the following stepwise method:
    a. We calculated the correlation network among all genes of the list using the Pearson's coefficient.
    b. For every gene, we calculated the mean Pearson's coefficient (*m*) and the mean of all the means (*M*).
    c. If *M*<*t*, we removed the gene with the smaller *m*.
    d. We repeated from step a. until *M*>=*t*.
5) This analysis led to a list of 31 robust *fibrous nest* genes and 25 robust *LF* genes. For *biliary/stem* genes, we used three biliary markers, known to be highly expressed in some HCCs, to correlate among them, and considered markers of a subtype of HCC expressing biliary features (*EPCAM, KRT19, SOX9*) (12-14).
6) To enrich these gene sets, we performed unsupervised analysis using all genes available in the metadata set. Among them, we selected those with a Pearson's coefficient >*t*, with at least one of the genes within the three gene sets. Then, they were added to the corresponding gene set, to reach 146 *fibrous nest*, 275 *liver fibrosis,* and 8 *biliary/stem*

genes. Then, the three gene sets were refined using the stepwise method described in 4). This led to the final gene sets: 48 robust *fibrous nest*, 32 robust *NT-liver fibrosis*, and 5 robust *biliary/stem* genes, showing a mean Pearson's coefficient of *t* (0.6 for *fibrous nest* and *NT-liver fibrosis*, and 0.5 for *biliary/stem*), between them. The 85 genes are shown in **Supplementary Table 3**.

Patient annotation using the three gene sets. First, 1,133 HCCs were classified by hierarchical clustering, based on expression of the three gene sets obtained in the previous step (n=85 genes), using Ward's method, and 1-Pearson correlation as a distance metric. This analysis presented in **Fig. 5B**, identified four groups of patients: *fibrous nest HCC*, *NT-liver fibrosis HCC*, *biliary/stem HCC*, and a group of intermediate phenotypes, showing a gradient of expression of the three networks. Patient annotation was determined by principal component analysis (PCA) **(Supplementary Fig. 8)**. In an additional step, we performed an individual reproducibility analysis, based on the method developed to identify our previously published four robust subclasses (5). We used the following steps:

1) To challenge the reproducibility of our classification, we generated alternative clustering using the same method but less than 85 genes. We gradually decreased the number of genes used from 84 to 40. At each step, we performed ten random draws of *n* genes, and generated dendrograms for each one, which generated 450 alternative dendrograms. Each dendrogram was split into four groups, and the annotation of every group was done using the clustering with 85 genes as a reference.
2) For each patient, we calculated the rate of affiliation to *fibrous nest*, *NT-liver fibrosis*, and *biliary/stem* among the 450 dendrograms. By comparing these numbers with the classification using 85 genes, we found that patients classified as *NT-liver fibrosis* had a mean rate of affiliation into the *LF* group >70%, among the 450 dendrograms. By contrast, patients classified as *fibrous nest* and *biliary/stem* had a mean rate of affiliation to their

group of 43%, and 57%, respectively. To improve patient annotation, we classified patients using the maximum rate of affiliation among the 450 dendrograms. For patients classified as intermediate, we did not change their annotation, unless the rate of annotation within the 450 dendrograms was >0.5 for one of the groups. With this new patient annotation, patients classified as *NT-liver fibrosis*, *fibrous nest*, and *biliary/stem* had a mean rate of affiliation to their group of 71%, 54%, and 59%, respectively. These three rates of affiliation were highly significant, based on permutation test ($p<10^{-3}$ each).

Integration of proteomics and transcriptomics analyses. Based on the results of proteomics and transcriptomics analyses of matrisome genes, several protein sets were identified using the criteria listed below.

Fibrous nest proteins fulfilled the following criteria:

1) By proteomics: increased in high- vs low-grade HCCs.
2) By transcriptomics: increased in *Fibrous nest* vs *NT-liver fibrosis* HCC (either in the metadata set or, if not available, in *GSE14520*).
3) By transcriptomics: in *Fibrous nest* HCCs from *GSE14520*, increased in T vs NT.

NT-liver fibrosis proteins fulfilled the following criteria:

1) By proteomics: in high-grade HCCs, decreased in T vs NT.
2) By proteomics: in low-grade HCCs, decreased in T vs NT.
3) By proteomics: not significantly increased in high- vs low-grade HCCs.
4) By transcriptomics: decreased in T vs NT (by combining the results of four DE analysis, as described in **Fig. 4A** and **Supplementary table 1**).

Common fibrosis proteins fulfilled the following criteria:

1) By proteomics: increased in high- vs low-grade HCCs.
2) By proteomics: in low-grade HCCs, decreased in T vs NT.
3) By proteomics: in high-grade HCCs, not significantly increased in T vs NT.

4) By transcriptomics: increased in *Fibrous nest* HCC vs *NT-liver fibrosis* HCC (either in the metadata set or, if not available, in *GSE14520*).
5) By transcriptomics: in *Fibrous nest* HCCs from *GSE14520*, not significantly increased in T vs NT.

Common HCC proteins fulfilled the following criteria:

1) By proteomics: in high-grade HCCs, increased in T vs NT.
2) By proteomics: in low-grade HCCs, increased in T vs NT.
3) By proteomics: not significantly increased in high- vs low-grade HCCs.

Low-grade HCC proteins fulfilled the following criteria:

1) By proteomics: in low-grade HCCs, increased in T vs NT.
2) By proteomics: in high-grade HCCs, not significantly increased in T vs NT.
3) By proteomics: decreased in high- vs low-grade HCCs.
4) By transcriptomics: decreased in *Fibrous nest* HCC vs *NT-liver fibrosis* HCC (either in the metadata set or, if not available, in *GSE14520*).

Analysis of the gene expression of the 27 *Fibrous nest* proteins in GSE14520, highlighted a correlation-based cluster of 11 genes, with high increase in gene expression in *Fibrous nest* HCC vs *NT-liver fibrosis* HCC (Fold change >5 for most of the genes) **(Fig. 8D)**. Hierarchical clustering-based clustering of the patients, using this 11-genes signature, allowed to capture most of the *Fibrous nest* HCC patients (83% of the *Fibrous nest* HCC and only 9% of the *NT-liver fibrosis* HCC, were assigned to this group). Univariate and multivariate Cox analyses were performed in combination with AFP, age, tumor size, and BCLC staging **(Fig. 8E)**.

Spatial cartography of matrisome biomarkers in HCC fibrous hotpots. Multiplexed immunohistochemical analyses were performed using Cell Dive technology (Leica Microsystems, Nanterre, France), and labeled primary antibodies **(Supplementary Table 7)**, at the

Histopathology High Precision facility, Rennes University (France). Fresh frozen HCC tissue cryosections (7 µm thick), were fixed for 10 min in 4% formalin, pH 7.4, at room temperature, rinsed in PBS, and permeabilized in 0.1% Triton-X100. The following steps were performed as per Cell Dive instructions: blocking unspecific binding was followed by DAPI staining, whole mount tissue imaging at 200x, quality control evaluation, and auto fluorescent imaging. Then, slides were de-coverslipped, washed with Tween wash buffer, labeled with the appropriate antibodies, washed, and images acquired at 200x. As four rounds of four antibodies were applied to the same whole mount HCC tissue blocks, slides were de-coverslipped between each round. The incubation medium was removed, and slides washed with Tween wash buffer, followed by quality control, imaging, dye inactivation, DAPI re-staining, washing, and a new antibody labeling round. Digital images were respectively acquired, and visualized with the Cell Dive and HALO (Indica Labs) imaging platforms, and artificially colored using color-blind-friendly RGB combinations.

Supplementary Figures

Supplementary Figure 1. Pie chart of the number of matrisome and non-matrisome proteins detected, semi quantitative value of the proteins determined by normalized total spectrum count, number of unique spectrum, and unique peptide counts, after qualitative proteomics, in four subsequent experiments, using different ECM enrichment protocols, in mouse or human liver fibrosis or HCC, followed by qualitative proteomics **(A-D)**. Venn diagram showing overlap in matrisome proteins in two human HCCs samples in duplicate, from experiment 4 **(E)**. Subcellular compartment of origin of proteins detected in the four experiments, based on the David platform (15) **(F)**. CCl_4, carbon tetrachloride; ECM, extracellular matrix; FDR, false discovery rate.

Supplementary Figure 2. Pie chart of the number of matrisome and non-matrisome proteins detected, semiquantitative value of the proteins determined by normalized total spectrum count, number of unique spectrum, and unique peptide counts, after TMT-MS based quantitative proteomics, in 12 mouse samples injected MO, CCl_4, or DEN. CCl_4, carbon tetrachloride; DEN, diethylnitrosamine; MO, mineral oil; MS, mass spectrometry; TMT, tandem mass tags.

Supplementary Figure 3. PCA plot based on abundance of the whole proteomics **(A)**, or of the 141 matrisome proteins **(B)**, in 12 samples from mice injected MO, CCl_4, or DEN. Venn diagram showing the number of proteins with significant difference in abundance among groups **(C)**. Heatmap of the differentially abundant matrisome proteins in mouse proteomics **(D)**. Validation of the mouse proteomics signature in publicly available transcriptomics data of the DEN model (16) by GSEA **(E)**. CCl_4, carbon tetrachloride; DEN, diethylnitrosamine; GSEA, gene set enrichment analysis; MO, mineral oil; PCA, principal component analysis.

Supplementary Figure 4. Pathway analysis of the proteins with significant difference in abundance between groups from mouse data, using the IPA platform **(A-C)**. Red, blue, and grey,

represent positive, negative, or non-available Z-scores, respectively, indicating positive or negative regulation of the pathway. Circle size represents overexpression of proteins in the signature. CCl_4, carbon tetrachloride; DEN, diethylnitrosamine; IPA, Ingenuity pathway analysis; MO, mineral oil; NT, non-tumor.

Supplementary Figure 5. Venn diagram showing overall changes between the matrisome of DEN-induced HCC in mice, and human HCC with high- or low-grade intratumor fibrosis. DEN, diethylnitrosamine.

Supplementary Figure 6. Pathway analysis of proteins with significant difference in abundance, between groups from human data, using the IPA platform **(A-F)**. Red, blue, and grey, represent positive, negative, or non-available Z-scores, respectively, indicating positive or negative regulation of the pathway. Circle size represents overexpression of proteins in the signature. IPA, Ingenuity pathway analysis; NT, non-tumor.

Supplementary Figure 7. Summary of upstream analysis using IPA. Red and blue represent positive and negative Z-scores, respectively, indicating positive or negative regulation of the downstream signaling pathways for any given upstream regulator. HCC, hepatocellular carcinoma; IPA, Ingenuity pathway analysis; NT, non-tumor.

Supplementary Figure 8. Venn diagram showing overlap between the proteins, with different abundance in high- compared to low-grade tumor fibrosis, in the tumor or in the NT tissue **(A-B)**. Summary of the comparison between groups of the 18 matrisome proteins, increased in tumor and decreased in NT tissue, in high- compared to low-grade tumor fibrosis **(C)**.

Supplementary Figure 9. Pathway analysis of proteins with significant difference in abundance, between groups from human data, using the IPA platform **(A-B)**. Red, blue, and grey, represent positive, negative, or non-available Z-scores, respectively, indicating positive or negative regulation of the pathway. Circle size represents overexpression of proteins in the signature. IPA, Ingenuity pathway analysis; NT, non-tumor.

Supplementary Figure 10. PCA plot based on expression of three gene sets (*NT-liver fibrosis*, *fibrous nest*, *biliary/stem*), in the 1,133 HCCs metadata set. The color of the group of patients reflects our previous HCC classification (5). Ellipses represent 95% confidence interval of the matrisome-based HCC classification. PCA, principal component analysis.

Supplementary Figure 11. Validation of the matrisome-based HCC classification in the TCGA cohort (n=294 HCCs), using hierarchical clustering, according to expression of *NT-liver fibrosis*, *fibrous nest* and *biliary/stem* genes (shown in green, red, and orange, respectively). Red: high expression; green: low expression.

Supplementary Figure 12. Venn diagram showing little overlap between proteins from high-grade fibrosis HCCs, and differentially expressed genes from *NT-liver fibrosis* **(A)**, and between proteins from low-grade fibrosis HCCs and differentially expressed genes from *fibrous nest HCCs* **(B).**

Supplementary Figure 13. Immunostaining of matrisome proteins from the fibrous nest signature, in an HCC sample with high-grade fibrosis visualized by multiplex imaging **(A-C).**

Supplementary Figure 14. Signatures of matrisome proteins showing different expression among groups, in the human matrisome analysis of HCCs and LF, as well as different gene

expression among groups in transcriptomics analysis **(A-D)**. Red: overexpression, blue: downregulation, grey: non-significant change, white: no available data. Human transcriptomics of T vs NT is based on the pipeline described in Fig. 1, or on the expression in the dataset from (21), after clustering patients as shown in Figs. 2 to 4. Expression in HCCs subclasses is based on analysis of either the 1,133 HCCs metadata set (when available), or the dataset shown in (21). Detailed criteria for protein selection are available in Supplementary Material and Methods.

Supplementary Figure 15. Venn diagram showing the overlap between the 27-proteins fibrous nest signature presented in Fig. 8C, and the Wnt3a signature obtained by in vitro treatment of HCC progenitor cells with recombinant Wnt3a (17) **(A)**. List of the 9 proteins overlapping the fibrous nest and the Wnt3a signatures **(B)**. Analysis of the Wnt3a signatures in the 1,133 HCC metadata set according to the matrisome based subclasses by GSEA **(C)**.

SUPPLEMENTARY TABLES

Supplementary Table 1. ***Baseline characteristics of patients with low- or high-grade intratumor fibrosis.***

Anony-mized Tumor ID	Anony-mized Non-Tumor ID	Inter-vention date	Age	Sex	Risk factors	Tumor size (cm)	Vascular invasion	Edmondson-Steiner's score	TNM staging	Capsule	FIBROSIS SCORE (0 - 1 - 2 - 3) Tumor	Tumor Fibrosis HG/LG	METAVIR Score (0 - 1 - 2 - 3 -4) Non-tumor
1	2	04/02/2008	75	M	alcohol/MS	8	1	3	T2NXM0	0	3	HG	2
25	26	18/05/2016	47	M	alcohol/MS			3	TXNXM0		3	HG	1
49	50	11/12/2001	62	M	alcohol	3	0	2	T2N0M0	0	2	HG	4
57	58	08/12/1997	50	M	alcohol/HC	4.4	1	3	T2N0M0	0	3	HG	4
59	60	02/09/1999	50	M	alcohol	3	1	3	T2N0M0	0	2	HG	4
61	62	29/11/1999	46	M	alcohol, HCV	3.5	0	2	T2N0M0	0	2	HG	4
63	64	20/03/2000	56	M	D2, dyslipidemia, tobacco	4	1	3	T2N0M0	0	3	HG	1
65	66	14/11/2001	73	M	alcohol	4.2	0	3	T2N0M0	0	3	HG	2
67	68	22/09/1999	68	M	alcohol	4	1	3	T2N0M0	0	3	HG	4
69	70	05/02/2001	74	M	alcohol	4.5	1	3	T2N0M0	0	3	HG	3
13	14	03/10/2011	55	M	alcohol/MS	24	1	2	T2NXM0	1	1	LG	3
15	16	27/10/2011	73	M	alcohol/MS	8	1	2	T2NXM0	0	1	LG	3
17	18	24/02/2014	72	M	alcohol/MS	9.5		2	T4NXM0	1	1	LG	4
41	42	11/05/1995	62	M	alcohol	7	1	3	T2N0M0	1	0	LG	4
43	44	04/04/2000	54	M	alcohol, HBV	3	0	3	T2N0M0	0	0	LG	4
45	46	18/01/2001	76	M	alcohol	3.8	1	2	T2N0M0	1	0	LG	3
47	48	03/07/2002	68	M	alcohol	3.5	0	2	T2N0M0	1	1	LG	4
51	52	06/08/2002	72	M	tobacco	3	0	2	T2N0M0	1	1 - 2	LG	3
53	54	22/05/2000	69	M	alcohol	3	0	2	T2N0M0	1	1 - 2	LG	3
55	56	25/06/2001	66	M	alcohol	10	0	2	T3N0M0	1	1	LG	4

Supplementary Table 2. ***Clinical comparison of high- vs low-grade intratumor fibrosis***

		Intratumor fibrosis		
	Missing value	**Low-grade (n=10)**	**High-grade (n=10)**	**p. value**
Age	0	66.7 +/- 7.53	60.1 +/- 11.73	0.27
Gender (Male)	0	10/10	10/10	1.00
BMI	4	28.17 +/- 4.11	27.7 +/- 3.81	0.87
Time to intervention date (days)	0	6911 +/- 2261	7441 +/- 2017	0.58
Etiology	0			0.64
Alcohol		5/10	5/10	
HBV		0/10	1/10	
Hemochromatosis		1/10	0/10	
HCV		1/10	0/10	
Metabolic syndrome		2/10	3/10	
Unknown		1/10	1/10	
AFP (UI/ml)	4	60.79 +/- 123.7	34.12 +/- 59.47	0.46
Liver transplantation*	0	1/10	3/10	0.58
Tumor size (cm)	1	7.48 +/- 6.44	4.29 +/- 1.5	0.56
Vascular invasion	2	4/9	6/9	0.64
Edmondson-Steiner score	0	2.2 +/- 0.42	2.8 +/- 0.42	**0.009**
TNM (T2)	0	8/10	9/10	1
TNM (N0)	0	7/10	8/10	1
TNM (M0)	0	10/10	10/10	1
Tumor necrosis	0	7/10	4/10	0.37
Capsule	1	8/10	0/9	**0.001**
METAVIR Score (in non-tumor)	0	3.5 +/- 0.53	2.9 +/- 1.29	0.41

* the rest of the patients had surgical resection

Supplementary Table 3. ***Publicly available transcriptomic datasets used for statistical analysis.***

Data source	Country of origin	Year	Platform description	Samples available	Reference
GSE25097	China	2011	Affymetrix Custom	258 T - 239 NT - 40 Cirrhosis	(18)
GSE14520	China	2010	Affymetrix U133A	237 T - 232 NT	(19)
GSE10143	Japan	2008	Illumina DNA–mediated annealing, select ion, extension, and ligation (DASL)	80 T - 307 NT	(20)
GSE17856	Japan	2010	Agilent-014850	42 T + 44 NT	(21)
TCGA - LIHC-US	USA-Asia-Russia-Canada-UK	2016	Illumina HiSeq	294 HCCs	(22)
HCC meta dataset from 9 publicly available datasets	Worldwide	2017	Multiple platforms	1,133 HCCs	(5)

Supplementary Table 4. ***Summary of all matrisome-based molecular patterns.***

Pattern name	T vs NT	ECM vs PP	STEM vs PP	Pattern annotation	N
Pattern 1	Up	Up	Up	Fibrous nest	88
Pattern 2	Down	Down	Down	NT liver fibrosis	87
Pattern 3	Down	Up	Up	Common fibrosis	66
Pattern 4	Down	Stable	Stable	NT liver fibrosis	51
Pattern 5	Down	Stable	Down	NT liver fibrosis	40
Pattern 6	Stable	Up	Up	Fibrous nest	32
Pattern 7	Down	Up	Stable	Common fibrosis	26
Pattern 8	Stable	Stable	Stable	Stable	23
Pattern 9	Down	Stable	Up	Common fibrosis	23
Pattern 10	Up	Stable	Stable	Tumor	18
Pattern 11	Up	Down	Down	Tumor	16
Pattern 12	Up	Up	Stable	Fibrous nest	14
Pattern 13	Stable	Stable	Down	Undetermined pattern	14
Pattern 14	Up	Stable	Up	Fibrous nest	14
Pattern 15	Stable	Down	Down	Undetermined pattern	11
Pattern 16	Stable	Up	Stable	ECM	8
Pattern 17	Down	Up	Down	ECM	7
Pattern 18	Down	Down	Stable	NT liver fibrosis	7
Pattern 19	Up	Stable	Down	Undetermined pattern	6
Pattern 20	Stable	Stable	Up	STEM	4
Pattern 21	Down	Down	Up	STEM	4
Pattern 22	Up	Down	Stable	Tumor	3
Pattern 23	Up	Up	Down	Undetermined pattern	2
Pattern 24	Stable	Down	Stable	NT liver fibrosis	1
Pattern 25	Stable	Up	Down	Undetermined pattern	1

Supplementary Table 5. ***Gene sets used for matrisome-based HCC classification.***

Gene symbol	Name	Cluster annotation	Matrisome gene
DCN	decorin	Fibrous nest	YES
LAMA2	laminin, alpha 2	Fibrous nest	YES
AEBP1	AE binding protein 1	Fibrous nest	YES
COL3A1	collagen, type III, alpha 1	Fibrous nest	YES
COL6A2	collagen, type VI, alpha 2	Fibrous nest	YES
COL6A3	collagen, type VI, alpha 3	Fibrous nest	YES
EFEMP1	EGF containing fibulin-like extracellular matrix protein 1	Fibrous nest	YES
MGP	matrix Gla protein	Fibrous nest	YES
MMP2	matrix metallopeptidase 2	Fibrous nest	YES
THBS2	thrombospondin 2	Fibrous nest	YES
TIMP1	TIMP metallopeptidase inhibitor 1	Fibrous nest	YES
SLIT2	slit homolog 2 (Drosophila)	Fibrous nest	YES
FSTL1	follistatin-like 1	Fibrous nest	YES
ASPN	asporin	Fibrous nest	YES
CRISPLD2	cysteine-rich secretory protein LCCL domain containing 2	Fibrous nest	YES
PLAT	plasminogen activator, tissue	Fibrous nest	YES
FBLN2	fibulin 2	Fibrous nest	YES
FBN1	fibrillin 1	Fibrous nest	YES
COL1A1	collagen, type I, alpha 1	Fibrous nest	YES
COL1A2	collagen, type I, alpha 2	Fibrous nest	YES
COL4A1	collagen, type IV, alpha 1	Fibrous nest	YES
COL4A2	collagen, type IV, alpha 2	Fibrous nest	YES
VCAN	versican	Fibrous nest	YES
POSTN	periostin, osteoblast specific factor	Fibrous nest	YES
EMILIN1	elastin microfibril interfacer 1	Fibrous nest	YES
SULF1	sulfatase 1	Fibrous nest	YES
MXRA5	matrix-remodelling associated 5	Fibrous nest	YES
ACTA2	actin, alpha 2, smooth muscle, aorta	Fibrous nest	NO
LRRC32	leucine rich repeat containing 32	Fibrous nest	NO
GAS1	growth arrest-specific 1	Fibrous nest	NO
GEM	GTP binding protein overexpressed in skeletal muscle	Fibrous nest	NO
ID4	inhibitor of DNA binding 4	Fibrous nest	NO
PDE1A	phosphodiesterase 1A, calmodulin-dependent	Fibrous nest	NO
PMP22	peripheral myelin protein 22	Fibrous nest	NO
PTGIS	prostaglandin I2 (prostacyclin) synthase	Fibrous nest	NO
THY1	Thy-1 cell surface antigen	Fibrous nest	NO
VIM	vimentin	Fibrous nest	NO

HEPH	hephaestin	Fibrous nest	NO
LHFP	lipoma HMGIC fusion partner	Fibrous nest	NO
MYL9	myosin, light chain 9, regulatory	Fibrous nest	NO
ADGRA2	NA	Fibrous nest	NO
DSE	dermatan sulfate epimerase	Fibrous nest	NO
LXN	latexin	Fibrous nest	NO
TUBB6	tubulin, beta 6 class V	Fibrous nest	NO
PTRF	polymerase I and transcript release factor	Fibrous nest	NO
FOXF1	forkhead box F1	Fibrous nest	NO
LUM	lumican	Fibrous nest	YES
SPARC	secreted protein, acidic, cysteine-rich (osteonectin)	Fibrous nest	YES
S100A14	S100 calcium binding protein A14	Biliary/stem	YES
EPCAM	epithelial cell adhesion molecule	Biliary/stem	NO
MAPK13	mitogen-activated protein kinase 13	Biliary/stem	NO
TMED3	transmembrane emp24 protein transport domain containing 3	Biliary/stem	NO
PRR15L	proline rich 15-like	Biliary/stem	NO
PLG	plasminogen	NT-liver fibrosis	YES
SERPINC1	serpin peptidase inhibitor, clade C (antithrombin), member 1	NT-liver fibrosis	YES
CCL16	chemokine (C-C motif) ligand 16	NT-liver fibrosis	YES
MASP2	mannan-binding lectin serine peptidase 2	NT-liver fibrosis	YES
APOC4	apolipoprotein C-IV	NT-liver fibrosis	NO
C8A	complement component 8, alpha polypeptide	NT-liver fibrosis	NO
CYP2J2	cytochrome P450, family 2, subfamily J, polypeptide 2	NT-liver fibrosis	NO
GYS2	glycogen synthase 2 (liver)	NT-liver fibrosis	NO
ABCB4	ATP-binding cassette, sub-family B (MDR/TAP), member 4	NT-liver fibrosis	NO
SLC10A1	solute carrier family 10, member 1	NT-liver fibrosis	NO
RDH16	retinol dehydrogenase 16 (all-trans)	NT-liver fibrosis	NO
SLC27A5	solute carrier family 27 (fatty acid transporter), member 5	NT-liver fibrosis	NO
ABAT	4-aminobutyrate aminotransferase	NT-liver fibrosis	NO
AQP9	aquaporin 9	NT-liver fibrosis	NO
BHMT	betaine--homocysteine S-methyltransferase	NT-liver fibrosis	NO
CYB5A	cytochrome b5 type A (microsomal)	NT-liver fibrosis	NO
DAO	D-amino-acid oxidase	NT-liver fibrosis	NO
EHHADH	enoyl-CoA, hydratase/3-hydroxyacyl CoA dehydrogenase	NT-liver fibrosis	NO
HAGH	hydroxyacylglutathione hydrolase	NT-liver fibrosis	NO
HPR	haptoglobin-related protein	NT-liver fibrosis	NO
OTC	ornithine carbamoyltransferase	NT-liver fibrosis	NO
PCK2	phosphoenolpyruvate carboxykinase 2 (mitochondrial)	NT-liver fibrosis	NO
PFKFB1	6-phosphofructo-2-kinase/fructose-2,6-biphosphatase 1	NT-liver fibrosis	NO
ALDH5A1	aldehyde dehydrogenase 5 family, member A1	NT-liver fibrosis	NO
CES2	carboxylesterase 2	NT-liver fibrosis	NO

NR1I3	nuclear receptor subfamily 1, group I, member 3	NT-liver fibrosis	NO
GLYAT	glycine-N-acyltransferase	NT-liver fibrosis	NO
ABCA6	ATP-binding cassette, sub-family A (ABC1), member 6	NT-liver fibrosis	NO
SEC14L2	SEC14-like 2 (S. cerevisiae)	NT-liver fibrosis	NO
DCXR	dicarbonyl/L-xylulose reductase	NT-liver fibrosis	NO
HAO1	hydroxyacid oxidase (glycolate oxidase) 1	NT-liver fibrosis	NO
ACSM5	acyl-CoA synthetase medium-chain family member 5	NT-liver fibrosis	NO

Supplementary Table 6. ***Gene set enrichment analysis of matrisome-based HCCs subclasses.***

Fibrous nest HCCs

NAME	SIZE	NES	NOM p-val	FDR q-val
HSIAO_HOUSEKEEPING_GENES	259	2.16	0.006	0.128
KIM_WT1_TARGETS_8HR_UP	128	2.08	0	0.187
LAIHO_COLORECTAL_CANCER_SERRATED_UP	78	2.05	0	0.178
CHARAFE_BREAST_CANCER_LUMINAL_VS_MESENCHYMAL_DN	297	2.02	0	0.18
AMUNDSON_POOR_SURVIVAL_AFTER_GAMMA_RADIATION_2G	129	1.99	0	0.232
WATANABE_RECTAL_CANCER_RADIOTHERAPY_RESPONSIVE_DN	73	1.98	0	0.21
APRELIKOVA_BRCA1_TARGETS	40	1.98	0	0.185
KEGG_FC_GAMMA_R_MEDIATED_PHAGOCYTOSIS	69	1.98	0	0.162
CHIARADONNA_NEOPLASTIC_TRANSFORMATION_KRAS_CDC25_UP	37	1.95	0	0.205
GU_PDEF_TARGETS_UP	58	1.95	0	0.193
NATSUME_RESPONSE_TO_INTERFERON_BETA_DN	32	1.95	0.002	0.184
AMIT_EGF_RESPONSE_480_HELA	121	1.94	0	0.173
GRUETZMANN_PANCREATIC_CANCER_UP	272	1.93	0	0.186
RODWELL_AGING_KIDNEY_UP	265	1.93	0	0.175
RAMASWAMY_METASTASIS_UP	43	1.92	0	0.176
FULCHER_INFLAMMATORY_RESPONSE_LECTIN_VS_LPS_UP	364	1.92	0	0.167
ZWANG_CLASS_2_TRANSIENTLY_INDUCED_BY_EGF	27	1.92	0	0.17
DIRMEIER_LMP1_RESPONSE_LATE_UP	45	1.91	0	0.166
GALLUZZI_PREVENT_MITOCHONDIAL_PERMEABILIZATION	16	1.91	0	0.164
NING_CHRONIC_OBSTRUCTIVE_PULMONARY_DISEASE_DN	77	1.91	0.002	0.157
REACTOME_AXON_GUIDANCE	177	1.91	0	0.152
REN_ALVEOLAR_RHABDOMYOSARCOMA_DN	336	1.90	0	0.151
RICKMAN_TUMOR_DIFFERENTIATED_MODERATELY_VS_POORLY_UP	69	1.90	0	0.151
VERHAAK_GLIOBLASTOMA_MESENCHYMAL	170	1.89	0	0.151
ISSAEVA_MLL2_TARGETS	51	1.89	0	0.154
REACTOME_L1CAM_INTERACTIONS	61	1.89	0.002	0.151
CHAUHAN_RESPONSE_TO_METHOXYESTRADIOL_DN	71	1.88	0.01	0.156
LIAO_METASTASIS	300	1.88	0	0.15
SASSON_RESPONSE_TO_GONADOTROPHINS_DN	65	1.88	0	0.147
KINSEY_TARGETS_OF_EWSR1_FLII_FUSION_DN	191	1.88	0	0.146
BASSO_CD40_SIGNALING_UP	78	1.88	0.002	0.141
HOSHIDA_LIVER_CANCER_SUBCLASS_S1	192	1.88	0	0.139
CHICAS_RB1_TARGETS_CONFLUENT	336	1.87	0	0.141
FOSTER_TOLERANT_MACROPHAGE_DN	247	1.87	0	0.144
PID_PDGFRB_PATHWAY	100	1.87	0.002	0.141
HOEBEKE_LYMPHOID_STEM_CELL_UP	59	1.87	0	0.139

PID_ILK_PATHWAY	33	1.86	0.004	0.143
REACTOME_SEMAPHORIN_INTERACTIONS	51	1.86	0	0.141
PARK_TRETINOIN_RESPONSE_AND_PML_RARA_FUSION	27	1.86	0.002	0.139
SWEET_KRAS_TARGETS_UP	63	1.86	0	0.137
DASU_IL6_SIGNALING_UP	47	1.86	0	0.134
HAHTOLA_MYCOSIS_FUNGOIDES_SKIN_UP	121	1.85	0	0.136
PHONG_TNF_RESPONSE_NOT_VIA_P38	257	1.85	0.002	0.138
SASSON_RESPONSE_TO_FORSKOLIN_DN	66	1.85	0	0.138
VANTVEER_BREAST_CANCER_ESR1_DN	159	1.85	0	0.135
LI_WILMS_TUMOR_VS_FETAL_KIDNEY_2_DN	43	1.85	0	0.133
AMUNDSON_POOR_SURVIVAL_AFTER_GAMMA_RADIATION_8G	77	1.84	0.002	0.132
LEI_MYB_TARGETS	238	1.84	0	0.13
HOSHIDA_LIVER_CANCER_SURVIVAL_UP	61	1.84	0	0.133
LEE_LIVER_CANCER_SURVIVAL_DN	112	1.84	0.004	0.134
PID_CXCR4_PATHWAY	76	1.83	0.002	0.139
DOUGLAS_BMI1_TARGETS_UP	339	1.83	0	0.137
LINDSTEDT_DENDRITIC_CELL_MATURATION_D	57	1.83	0	0.135
HEIDENBLAD_AMPLICON_12P11_12_UP	23	1.83	0	0.133
DACOSTA_UV_RESPONSE_VIA_ERCC3_XPCS_DN	61	1.83	0.006	0.131
HUANG_DASATINIB_RESISTANCE_UP	58	1.83	0.004	0.13
FRIDMAN_IMMORTALIZATION_DN	25	1.83	0.002	0.128
TSAI_RESPONSE_TO_IONIZING_RADIATION	115	1.83	0.006	0.127
ROZANOV_MMP14_TARGETS_SUBSET	26	1.83	0	0.126
MILI_PSEUDOPODIA_HAPTOTAXIS_DN	382	1.83	0.004	0.125
FERRANDO_T_ALL_WITH_MLL_ENL_FUSION_UP	62	1.83	0.004	0.123
TSENG_IRS1_TARGETS_UP	74	1.83	0.002	0.123
HINATA_NFKB_TARGETS_FIBROBLAST_UP	68	1.82	0	0.124
YAGI_AML_WITH_T_8_21_TRANSLOCATION	261	1.82	0	0.122
QI_PLASMACYTOMA_DN	71	1.82	0.004	0.121
REACTOME_SIGNALING_BY_PDGF	89	1.82	0	0.119
PASINI_SUZ12_TARGETS_DN	213	1.82	0	0.118
GALINDO_IMMUNE_RESPONSE_TO_ENTEROTOXIN	65	1.82	0.004	0.117
COULOUARN_TEMPORAL_TGFB1_SIGNATURE_UP	71	1.82	0	0.117
BURTON_ADIPOGENESIS_11	36	1.82	0.006	0.116
PETROVA_ENDOTHELIUM_LYMPHATIC_VS_BLOOD_DN	129	1.82	0	0.116
KRIEG_HYPOXIA_NOT_VIA_KDM3A	420	1.82	0	0.114
SESTO_RESPONSE_TO_UV_C8	59	1.82	0	0.113
BURTON_ADIPOGENESIS_8	53	1.82	0	0.113
KEGG_FOCAL_ADHESION	151	1.82	0.002	0.112
HIRSCH_CELLULAR_TRANSFORMATION_SIGNATURE_UP	193	1.82	0.004	0.111
CHARAFE_BREAST_CANCER_BASAL_VS_MESENCHYMAL_DN	30	1.81	0	0.112

MARTENS_BOUND_BY_PML_RARA_FUSION	264	1.81	0.004	0.111
MORI_IMMATURE_B_LYMPHOCYTE_UP	37	1.81	0.006	0.111
PID_AP1_PATHWAY	54	1.81	0	0.11
KIM_WT1_TARGETS_UP	159	1.81	0	0.109
BENPORATH_ES_CORE_NINE_CORRELATED	81	1.81	0	0.109
THEILGAARD_NEUTROPHIL_AT_SKIN_WOUND_DN	169	1.81	0.002	0.11
GERHOLD_ADIPOGENESIS_DN	52	1.81	0	0.109
LINDGREN_BLADDER_CANCER_CLUSTER_2B	268	1.81	0	0.11
SIG_REGULATION_OF_THE_ACTIN_CYTOSKELETON_BY_RHO_GTPASES	25	1.81	0.004	0.109
FAELT_B_CLL_WITH_VH_REARRANGEMENTS_UP	32	1.81	0.008	0.107
RUTELLA_RESPONSE_TO_HGF_DN	169	1.81	0.006	0.107
PID_FRA_PATHWAY	32	1.80	0.002	0.108
FRIDMAN_SENESCENCE_UP	69	1.80	0.006	0.108
PHONG_TNF_RESPONSE_VIA_P38_PARTIAL	136	1.80	0	0.108
REACTOME_MYD88_MAL_CASCADE_INITIATED_ON_PLASMA_MEMBRANE	59	1.80	0.002	0.107
ST_T_CELL_SIGNAL_TRANSDUCTION	34	1.80	0.012	0.106
KYNG_ENVIRONMENTAL_STRESS_RESPONSE_NOT_BY_4NQO_IN_WS	26	1.80	0.006	0.106
VERRECCHIA_DELAYED_RESPONSE_TO_TGFB1	29	1.80	0.002	0.105
MILI_PSEUDOPODIA_CHEMOTAXIS_DN	296	1.80	0.002	0.105
CHARAFE_BREAST_CANCER_LUMINAL_VS_BASAL_DN	298	1.80	0	0.104
ZHANG_ANTIVIRAL_RESPONSE_TO_RIBAVIRIN_DN	40	1.80	0	0.104
JIANG_AGING_CEREBRAL_CORTEX_DN	32	1.80	0.004	0.105
DAVICIONI_MOLECULAR_ARMS_VS_ERMS_DN	127	1.80	0.004	0.104
RICKMAN_TUMOR_DIFFERENTIATED_WELL_VS_POORLY_DN	209	1.80	0.006	0.103
ST_INTEGRIN_SIGNALING_PATHWAY	62	1.80	0	0.103
PHONG_TNF_TARGETS_UP	51	1.80	0.002	0.102
NEMETH_INFLAMMATORY_RESPONSE_LPS_UP	68	1.79	0.002	0.101
NGUYEN_NOTCH1_TARGETS_DN	61	1.79	0.002	0.101
CHIARADONNA_NEOPLASTIC_TRANSFORMATION_KRAS_UP	93	1.79	0	0.101
KEGG_EPITHELIAL_CELL_SIGNALING_IN_HELICOBACTER_PYLORI_INFECTION	47	1.79	0.004	0.101
VART_KSHV_INFECTION_ANGIOGENIC_MARKERS_UP	119	1.79	0.002	0.101
LINDVALL_IMMORTALIZED_BY_TERT_UP	56	1.79	0	0.1
RUTELLA_RESPONSE_TO_HGF_VS_CSF2RB_AND_IL4_DN	176	1.79	0.002	0.1
SAFFORD_T_LYMPHOCYTE_ANERGY	60	1.79	0	0.1
KARLSSON_TGFB1_TARGETS_UP	76	1.79	0.006	0.1
WIERENGA_STAT5A_TARGETS_DN	121	1.79	0	0.099
SERVITJA_ISLET_HNF1A_TARGETS_UP	120	1.79	0	0.098
HUANG_GATA2_TARGETS_UP	95	1.79	0.01	0.1
LIM_MAMMARY_STEM_CELL_UP	277	1.79	0.002	0.1
HOSHIDA_LIVER_CANCER_LATE_RECURRENCE_UP	43	1.78	0	0.1
KEGG_SMALL_CELL_LUNG_CANCER	72	1.78	0	0.1

DANG_REGULATED_BY_MYC_DN	195	1.78	0	0.102
CROMER_TUMORIGENESIS_UP	48	1.78	0	0.102
BAELDE_DIABETIC_NEPHROPATHY_DN	333	1.78	0.004	0.102
VANHARANTA_UTERINE_FIBROID_UP	36	1.78	0.002	0.102
WORSCHECH_TUMOR_EVASION_AND_TOLEROGENICITY_UP	21	1.78	0.002	0.103
REACTOME_INTEGRIN_CELL_SURFACE_INTERACTIONS	65	1.78	0	0.102
SESTO_RESPONSE_TO_UV_C3	16	1.78	0.006	0.102
REACTOME_MAPK_TARGETS_NUCLEAR_EVENTS_MEDIATED_BY_MAP_KINASES	27	1.78	0.004	0.101
MCBRYAN_PUBERTAL_TGFB1_TARGETS_UP	132	1.78	0.002	0.101
PECE_MAMMARY_STEM_CELL_DN	77	1.78	0.006	0.101
HOFFMANN_IMMATURE_TO_MATURE_B_LYMPHOCYTE_UP	30	1.77	0.008	0.101
BENPORATH_NOS_TARGETS	111	1.77	0	0.1
VECCHI_GASTRIC_CANCER_ADVANCED_VS_EARLY_UP	113	1.77	0	0.099
BERENJENO_ROCK_SIGNALING_NOT_VIA_RHOA_DN	34	1.77	0.006	0.099
PID_INTEGRIN3_PATHWAY	34	1.77	0.004	0.098
URS_ADIPOCYTE_DIFFERENTIATION_DN	20	1.77	0	0.097
DAVICIONI_TARGETS_OF_PAX_FOXO1_FUSIONS_UP	196	1.77	0	0.097
GOTZMANN_EPITHELIAL_TO_MESENCHYMAL_TRANSITION_UP	59	1.77	0	0.096
MORI_MATURE_B_LYMPHOCYTE_UP	60	1.77	0.016	0.096
LANG_MYB_FAMILY_TARGETS	20	1.77	0.014	0.096
JOHANSSON_GLIOMAGENESIS_BY_PDGFB_UP	44	1.77	0.014	0.096
GENTILE_UV_RESPONSE_CLUSTER_D1	15	1.77	0	0.095
KEGG_PATHOGENIC_ESCHERICHIA_COLI_INFECTION	33	1.77	0.004	0.095
THEILGAARD_NEUTROPHIL_AT_SKIN_WOUND_UP	57	1.77	0.006	0.095
DELACROIX_RARG_BOUND_MEF	216	1.77	0	0.094
NAKAMURA_TUMOR_ZONE_PERIPHERAL_VS_CENTRAL_UP	172	1.77	0	0.094
DELYS_THYROID_CANCER_UP	343	1.77	0	0.093
LINDSTEDT_DENDRITIC_CELL_MATURATION_C	53	1.77	0	0.093
ZHAN_EARLY_DIFFERENTIATION_GENES_DN	34	1.77	0.004	0.093
IGLESIAS_E2F_TARGETS_UP	116	1.77	0.004	0.092
GENTILE_UV_HIGH_DOSE_DN	235	1.77	0.002	0.092
MIYAGAWA_TARGETS_OF_EWSR1_ETS_FUSIONS_DN	133	1.77	0	0.092
PID_NOTCH_PATHWAY	40	1.77	0	0.092
SCHUETZ_BREAST_CANCER_DUCTAL_INVASIVE_UP	270	1.77	0	0.092
SCHOEN_NFKB_SIGNALING	26	1.77	0	0.092
BILD_HRAS_ONCOGENIC_SIGNATURE	161	1.77	0.004	0.092
REACTOME_P75_NTR_RECEPTOR_MEDIATED_SIGNALLING	61	1.77	0.004	0.091
CAIRO_LIVER_DEVELOPMENT_UP	125	1.77	0.002	0.091
KEGG_NOD_LIKE_RECEPTOR_SIGNALING_PATHWAY	37	1.77	0.006	0.09
TAKEDA_TARGETS_OF_NUP98_HOXA9_FUSION_6HR_DN	25	1.77	0.002	0.089
CHICAS_RB1_TARGETS_SENESCENT	347	1.76	0	0.089

OSWALD_HEMATOPOIETIC_STEM_CELL_IN_COLLAGEN_GEL_UP	170	1.76	0.004	0.089
DANG_MYC_TARGETS_DN	25	1.76	0	0.089
MARCHINI_TRABECTEDIN_RESISTANCE_DN	40	1.76	0.006	0.089
NAKAMURA_ADIPOGENESIS_LATE_DN	28	1.76	0	0.089
TURASHVILI_BREAST_DUCTAL_CARCINOMA_VS_LOBULAR_NORMAL_UP	44	1.76	0	0.088
ZHANG_BREAST_CANCER_PROGENITORS_DN	91	1.76	0.002	0.088
REACTOME_CTLA4_INHIBITORY_SIGNALING	20	1.76	0.012	0.088
DORN_ADENOVIRUS_INFECTION_24HR_DN	31	1.76	0.01	0.089
KHETCHOUMIAN_TRIM24_TARGETS_UP	39	1.76	0	0.089
KYNG_ENVIRONMENTAL_STRESS_RESPONSE_NOT_BY_GAMMA_IN_OLD	21	1.76	0.006	0.089
RUTELLA_RESPONSE_TO_CSF2RB_AND_IL4_UP	257	1.76	0.004	0.088
HASLINGER_B_CLL_WITH_11Q23_DELETION	17	1.76	0.004	0.089
GENTILE_UV_LOW_DOSE_DN	52	1.76	0.006	0.088
WIERENGA_STAT5A_TARGETS_GROUP2	39	1.76	0	0.088
BURTON_ADIPOGENESIS_9	64	1.76	0	0.088
KEGG_RENAL_CELL_CARCINOMA	54	1.76	0.008	0.088
SCHAEFFER_PROSTATE_DEVELOPMENT_48HR_DN	236	1.76	0	0.088
ZHANG_RESPONSE_TO_CANTHARIDIN_UP	16	1.76	0.01	0.088
BASSO_HAIRY_CELL_LEUKEMIA_DN	58	1.76	0.002	0.087
REACTOME_CELL_SURFACE_INTERACTIONS_AT_THE_VASCULAR_WALL	72	1.76	0.004	0.087
TONKS_TARGETS_OF_RUNX1_RUNX1T1_FUSION_HSC_UP	146	1.76	0	0.086
KIM_WT1_TARGETS_12HR_UP	122	1.76	0.002	0.086
MULLIGHAN_MLL_SIGNATURE_2_DN	198	1.76	0.004	0.086
CHIARADONNA_NEOPLASTIC_TRANSFORMATION_KRAS_DN	106	1.75	0.002	0.086
AMUNDSON_GENOTOXIC_SIGNATURE	74	1.75	0	0.086
LIEN_BREAST_CARCINOMA_METAPLASTIC_VS_DUCTAL_UP	62	1.75	0	0.085
PID_FCER1_PATHWAY	49	1.75	0.012	0.086
CHIARADONNA_NEOPLASTIC_TRANSFORMATION_CDC25_DN	110	1.75	0.002	0.085
PID_INTEGRIN1_PATHWAY	52	1.75	0.002	0.085
JACKSON_DNMT1_TARGETS_UP	63	1.75	0.004	0.085
WAMUNYOKOLI_OVARIAN_CANCER_LMP_DN	126	1.75	0.002	0.084
PID_AVB3_INTEGRIN_PATHWAY	55	1.75	0.002	0.084
OLSSON_E2F3_TARGETS_UP	19	1.75	0.008	0.084
REACTOME_NCAM_SIGNALING_FOR_NEURITE_OUT_GROWTH	45	1.75	0.002	0.084
PID_SYNDECAN_1_PATHWAY	36	1.75	0	0.084
LI_AMPLIFIED_IN_LUNG_CANCER	130	1.75	0.006	0.084
YAGI_AML_FAB_MARKERS	146	1.75	0	0.084
LINDSTEDT_DENDRITIC_CELL_MATURATION_A	53	1.75	0	0.084
BROCKE_APOPTOSIS_REVERSED_BY_IL6	102	1.75	0.008	0.084
SANA_RESPONSE_TO_IFNG_DN	55	1.75	0.008	0.083
HENDRICKS_SMARCA4_TARGETS_UP	37	1.75	0.006	0.083

BENPORATH_OCT4_TARGETS	187	1.75	0.002	0.084
AMIT_EGF_RESPONSE_120_MCF10A	35	1.75	0.014	0.083
NADLER_OBESITY_UP	47	1.75	0.002	0.083
REACTOME_EXTRACELLULAR_MATRIX_ORGANIZATION	56	1.75	0	0.082
KYNG_ENVIRONMENTAL_STRESS_RESPONSE_NOT_BY_GAMMA_IN_WS	23	1.75	0.006	0.082
HINATA_NFKB_TARGETS_KERATINOCYTE_UP	74	1.75	0.006	0.082
REACTOME_ERK_MAPK_TARGETS	18	1.75	0.012	0.082
ROSS_AML_WITH_CBFB_MYH11_FUSION	42	1.74	0.006	0.083
DIAZ_CHRONIC_MEYLOGENOUS_LEUKEMIA_DN	88	1.74	0.006	0.083
VILIMAS_NOTCH1_TARGETS_UP	42	1.74	0.004	0.083
QI_PLASMACYTOMA_UP	191	1.74	0.024	0.083
ELVIDGE_HYPOXIA_UP	124	1.74	0.004	0.083
WANG_ESOPHAGUS_CANCER_VS_NORMAL_UP	87	1.74	0	0.083
KEGG_PATHWAYS_IN_CANCER	249	1.74	0	0.083
KYNG_RESPONSE_TO_H2O2	50	1.74	0.016	0.083
JECHLINGER_EPITHELIAL_TO_MESENCHYMAL_TRANSITION_UP	60	1.74	0	0.083
CHIARETTI_ACUTE_LYMPHOBLASTIC_LEUKEMIA_ZAP70	46	1.74	0	0.082
REACTOME_NUCLEAR_EVENTS_KINASE_AND_TRANSCRIPTION_FACTOR_ACTIVATION	21	1.74	0.014	0.082
VERRECCHIA_EARLY_RESPONSE_TO_TGFB1	43	1.74	0.006	0.082
TONKS_TARGETS_OF_RUNX1_RUNX1T1_FUSION_ERYTHROCYTE_UP	126	1.74	0.006	0.083
POOLA_INVASIVE_BREAST_CANCER_UP	208	1.74	0.002	0.082
WANG_SMARCE1_TARGETS_UP	160	1.74	0	0.083
KEGG_NOTCH_SIGNALING_PATHWAY	26	1.74	0.018	0.083
TONKS_TARGETS_OF_RUNX1_RUNX1T1_FUSION_MONOCYTE_UP	132	1.74	0.01	0.082
PID_AVB3_OPN_PATHWAY	27	1.74	0	0.083
SENESE_HDAC1_AND_HDAC2_TARGETS_UP	150	1.74	0.002	0.083
MCLACHLAN_DENTAL_CARIES_UP	190	1.74	0.008	0.083
CHEN_HOXA5_TARGETS_9HR_DN	30	1.73	0.004	0.083
PID_ENDOTHELIN_PATHWAY	51	1.73	0	0.083
FLOTHO_PEDIATRIC_ALL_THERAPY_RESPONSE_UP	39	1.73	0.031	0.082
PID_RAC1_PATHWAY	40	1.73	0.004	0.082
BARIS_THYROID_CANCER_DN	45	1.73	0.006	0.082
KIM_GLIS2_TARGETS_UP	64	1.73	0	0.082
LIU_TARGETS_OF_VMYB_VS_CMYB_DN	26	1.73	0.002	0.082
LINDGREN_BLADDER_CANCER_CLUSTER_3_DN	131	1.73	0.002	0.082
CASORELLI_ACUTE_PROMYELOCYTIC_LEUKEMIA_UP	116	1.73	0.004	0.082
LU_TUMOR_ANGIOGENESIS_UP	21	1.73	0	0.082
MARZEC_IL2_SIGNALING_UP	84	1.73	0.004	0.081
VERHAAK_AML_WITH_NPM1_MUTATED_DN	174	1.73	0	0.082
CROMER_METASTASIS_UP	57	1.73	0.008	0.083
GAVIN_FOXP3_TARGETS_CLUSTER_P3	94	1.73	0.004	0.083

RODWELL_AGING_KIDNEY_NO_BLOOD_UP	124	1.73	0.004	0.083
KYNG_ENVIRONMENTAL_STRESS_RESPONSE_UP	40	1.73	0.014	0.083
VALK_AML_CLUSTER_12	19	1.73	0.004	0.083
STEARMAN_LUNG_CANCER_EARLY_VS_LATE_DN	45	1.73	0.01	0.083
NABA_CORE_MATRISOME	143	1.73	0	0.083
LIAN_LIPA_TARGETS_6M	45	1.73	0.012	0.083
ROSS_ACUTE_MYELOID_LEUKEMIA_CBF	58	1.73	0.002	0.083
BURTON_ADIPOGENESIS_7	38	1.73	0.006	0.082
NABA_ECM_GLYCOPROTEINS	101	1.73	0.004	0.082
HUPER_BREAST_BASAL_VS_LUMINAL_DN	40	1.73	0.006	0.082
LEONARD_HYPOXIA	36	1.72	0.008	0.082
SASAI_RESISTANCE_TO_NEOPLASTIC_TRANSFROMATION	39	1.72	0.004	0.082
WOO_LIVER_CANCER_RECURRENCE_UP	83	1.72	0	0.081
XU_HGF_SIGNALING_NOT_VIA_AKT1_48HR_UP	29	1.72	0.002	0.082
KEGG_LEISHMANIA_INFECTION	49	1.72	0.006	0.082
HARRIS_HYPOXIA	62	1.72	0.002	0.082
REACTOME_SIGNALLING_TO_ERKS	24	1.72	0.01	0.081
LA_MEN1_TARGETS	17	1.72	0.004	0.081
MORI_LARGE_PRE_BII_LYMPHOCYTE_DN	40	1.72	0.028	0.081
PID_P53_DOWNSTREAM_PATHWAY	97	1.72	0.004	0.081
TURASHVILI_BREAST_LOBULAR_CARCINOMA_VS_DUCTAL_NORMAL_UP	45	1.72	0	0.081
NABA_BASEMENT_MEMBRANES	25	1.72	0.006	0.081
STONER_ESOPHAGEAL_CARCINOGENESIS_UP	23	1.72	0.013	0.081
RICKMAN_METASTASIS_DN	157	1.72	0.019	0.081
SA_B_CELL_RECEPTOR_COMPLEXES	22	1.72	0.01	0.081
QI_HYPOXIA_TARGETS_OF_HIF1A_AND_FOXA2	26	1.72	0.016	0.081
KOYAMA_SEMA3B_TARGETS_UP	146	1.72	0.004	0.081
AMIT_SERUM_RESPONSE_60_MCF10A	43	1.72	0.004	0.081
PETROVA_PROX1_TARGETS_DN	52	1.72	0.002	0.081
HANN_RESISTANCE_TO_BCL2_INHIBITOR_UP	25	1.72	0.004	0.08
KIM_WT1_TARGETS_12HR_DN	154	1.72	0.002	0.08
MARKEY_RB1_CHRONIC_LOF_DN	79	1.72	0.006	0.08
MUNSHI_MULTIPLE_MYELOMA_UP	59	1.72	0.01	0.08
REACTOME_PROTEIN_FOLDING	27	1.72	0.017	0.079
SIG_PIP3_SIGNALING_IN_B_LYMPHOCYTES	28	1.72	0.006	0.079
PID_RHOA_REG_PATHWAY	33	1.72	0.014	0.079
WONG_ADULT_TISSUE_STEM_MODULE	477	1.72	0	0.079
BASSO_B_LYMPHOCYTE_NETWORK	96	1.72	0.014	0.079
CROONQUIST_NRAS_VS_STROMAL_STIMULATION_DN	71	1.72	0.01	0.079
REACTOME_SIGNALING_BY_RHO_GTPASES	72	1.72	0.004	0.079
LENAOUR_DENDRITIC_CELL_MATURATION_DN	95	1.72	0.024	0.079

BOUDOUKHA_BOUND_BY_IGF2BP2	73	1.71	0.014	0.081
RUTELLA_RESPONSE_TO_CSF2RB_AND_IL4_DN	224	1.71	0.018	0.081
RUTELLA_RESPONSE_TO_HGF_VS_CSF2RB_AND_IL4_UP	305	1.71	0.012	0.081
PID_IL8_CXCR2_PATHWAY	24	1.71	0.014	0.081
TURASHVILI_BREAST_LOBULAR_CARCINOMA_VS_LOBULAR_NORMAL_DN	43	1.71	0	0.08
AMIT_EGF_RESPONSE_40_HELA	32	1.71	0.019	0.08
PARK_HSC_MARKERS	27	1.71	0.012	0.08
SMID_BREAST_CANCER_BASAL_UP	465	1.71	0	0.08
DACOSTA_ERCC3_ALLELE_XPCS_VS_TTD_DN	28	1.71	0	0.08
GUENTHER_GROWTH_SPHERICAL_VS_ADHERENT_DN	23	1.71	0.012	0.08
PID_ALPHA_SYNUCLEIN_PATHWAY	25	1.71	0.016	0.08
GAZDA_DIAMOND_BLACKFAN_ANEMIA_PROGENITOR_UP	29	1.71	0.004	0.079
KORKOLA_EMBRYONAL_CARCINOMA_UP	25	1.71	0.004	0.079
REACTOME_MAP_KINASE_ACTIVATION_IN_TLR_CASCADE	35	1.71	0.01	0.079
WEI_MIR34A_TARGETS	98	1.71	0.002	0.079
CUI_TCF21_TARGETS_2_UP	243	1.71	0.002	0.079
JOHNSTONE_PARVB_TARGETS_3_UP	273	1.71	0.004	0.079
WIERENGA_STAT5A_TARGETS_UP	116	1.71	0.01	0.079
MORI_SMALL_PRE_BII_LYMPHOCYTE_DN	52	1.71	0.014	0.079
RUTELLA_RESPONSE_TO_HGF_UP	312	1.71	0.006	0.079
GOLDRATH_ANTIGEN_RESPONSE	226	1.71	0.014	0.079
HENDRICKS_SMARCA4_TARGETS_DN	30	1.71	0.01	0.079
SENESE_HDAC3_TARGETS_UP	319	1.71	0.002	0.08
REACTOME_COLLAGEN_FORMATION	37	1.71	0	0.08
ALTEMEIER_RESPONSE_TO_LPS_WITH_MECHANICAL_VENTILATION	92	1.70	0.016	0.081
BIOCARTA_FAS_PATHWAY	26	1.70	0.026	0.081
KRIGE_RESPONSE_TO_TOSEDOSTAT_24HR_UP	420	1.70	0.004	0.08
ACEVEDO_LIVER_CANCER_WITH_H3K27ME3_UP	137	1.70	0	0.08
HOLLMANN_APOPTOSIS_VIA_CD40_DN	194	1.70	0.004	0.08
PID_CASPASE_PATHWAY	41	1.70	0.015	0.081
WILCOX_RESPONSE_TO_PROGESTERONE_DN	46	1.70	0	0.08
REACTOME_TOLL_RECEPTOR_CASCADES	84	1.70	0.025	0.08
PID_RHOA_PATHWAY	31	1.70	0.013	0.08
MARKEY_RB1_ACUTE_LOF_DN	145	1.70	0.022	0.08
DITTMER_PTHLH_TARGETS_UP	89	1.70	0.014	0.08
GILDEA_METASTASIS	23	1.70	0.002	0.08
JIANG_HYPOXIA_NORMAL	216	1.70	0.006	0.08
HELLER_HDAC_TARGETS_SILENCED_BY_METHYLATION_DN	190	1.70	0.004	0.08
KEGG_T_CELL_RECEPTOR_SIGNALING_PATHWAY	87	1.70	0.04	0.08
KEGG_ECM_RECEPTOR_INTERACTION	65	1.70	0.006	0.08
LIU_PROSTATE_CANCER_DN	278	1.70	0.004	0.079

Biliary/stem HCCs

NAME	SIZE	NES	NOM p-val	FDR q-val
REACTOME_INFLUENZA_LIFE_CYCLE	79	2.33	0	0.003549
HOSHIDA_LIVER_CANCER_SUBCLASS_S2	89	2.24	0	0.004561
REACTOME_MRNA_PROCESSING	91	2.23	0	0.003041
REACTOME_PROCESSING_OF_CAPPED_INTRON_CONTAINING_PRE_MRNA	80	2.20	0	0.003506
REACTOME_TRANSLATION	77	2.19	0	0.00425
CAIRO_HEPATOBLASTOMA_CLASSES_UP	428	2.15	0	0.008503
BOYAULT_LIVER_CANCER_SUBCLASS_G1_UP	77	2.14	0	0.007523
ZHAN_VARIABLE_EARLY_DIFFERENTIATION_GENES_DN	25	2.11	0	0.009333
REACTOME_LATE_PHASE_OF_HIV_LIFE_CYCLE	74	2.11	0.004049	0.008993
REACTOME_MRNA_SPLICING_MINOR_PATHWAY	27	2.09	0	0.010498
REACTOME_METABOLISM_OF_NON_CODING_RNA	31	2.06	0	0.014141
REACTOME_HIV_LIFE_CYCLE	84	2.05	0.003968	0.015093
CAIRO_HEPATOBLASTOMA_UP	146	2.02	0	0.019824
REACTOME_NEP_NS2_INTERACTS_WITH_THE_CELLULAR_EXPORT_MACHINERY	23	2.01	0	0.019607
REACTOME_TRANSPORT_OF_RIBONUCLEOPROTEINS_INTO_THE_HOST_NUCLEUS	22	2.00	0	0.019855
REACTOME_INFLUENZA_VIRAL_RNA_TRANSCRIPTION_AND_REPLICATION	52	1.99	0.008097	0.022464
REACTOME_INTERACTIONS_OF_VPR_WITH_HOST_CELLULAR_PROTEINS	24	1.98	0	0.0239
REACTOME_METABOLISM_OF_RNA	161	1.98	0.00789	0.023629
REACTOME_SIGNALING_BY_NOTCH1	42	1.96	0.00202	0.028394
REACTOME_RNA_POL_III_TRANSCRIPTION_INITIATION_FROM_TYPE_2_PROMOTER	17	1.95	0.004107	0.032927
REACTOME_SRP_DEPENDENT_COTRANSLATIONAL_PROTEIN_TARGETING_TO_MEMBRANE	56	1.95	0.006198	0.032158
BILANGES_SERUM_RESPONSE_TRANSLATION	18	1.93	0.002101	0.038195
KEGG_SPLICEOSOME	72	1.92	0.009921	0.039084
BOYAULT_LIVER_CANCER_SUBCLASS_G123_UP	32	1.92	0	0.041391
REACTOME_MRNA_SPLICING	55	1.92	0.009921	0.040361
REACTOME_3_UTR_MEDIATED_TRANSLATIONAL_REGULATION	49	1.91	0.006135	0.041122
GINESTIER_BREAST_CANCER_ZNF217_AMPLIFIED_DN	166	1.91	0.012658	0.039773
SCHLOSSER_MYC_TARGETS_AND_SERUM_RESPONSE_UP	34	1.91	0.002088	0.041121
RICKMAN_TUMOR_DIFFERENTIATED_WELL_VS_POORLY_UP	135	1.91	0	0.039952
KEGG_NOTCH_SIGNALING_PATHWAY	26	1.89	0.002083	0.047558
PATIL_LIVER_CANCER	458	1.89	0.005758	0.047108
BOYAULT_LIVER_CANCER_SUBCLASS_G12_UP	32	1.88	0.003929	0.050323
REACTOME_RNA_POL_II_PRE_TRANSCRIPTION_EVENTS	41	1.88	0.018145	0.049839
REACTOME_ELONGATION_ARREST_AND_RECOVERY	23	1.88	0.004024	0.048598
REACTOME_SIGNALING_BY_NOTCH	63	1.88	0.006085	0.04836
DEN_INTERACT_WITH_LCA5	19	1.87	0.007692	0.04975

REACTOME_DOWNREGULATION_OF_SMAD2_3_SMAD4_TRANSCRIPTIONAL_ACTIVITY	16	1.87	0.006	0.051674
REACTOME_RNA_POL_III_TRANSCRIPTION_INITIATION_FROM_TYPE_3_PROMOTER	19	1.85	0.010526	0.065462
AIYAR_COBRA1_TARGETS_DN	20	1.84	0	0.06507
WELCSH_BRCA1_TARGETS_DN	98	1.84	0.005952	0.064671
REACTOME_FORMATION_OF_RNA_POL_II_ELONGATION_COMPLEX_	30	1.83	0.020161	0.070859
RHODES_CANCER_META_SIGNATURE	42	1.83	0.005988	0.069312
REACTOME_MICRORNA_MIRNA_BIOGENESIS	17	1.83	0.019763	0.067772
REACTOME_ABORTIVE_ELONGATION_OF_HIV1_TRANSCRIPT_IN_THE_ABSENCE_OF_TAT	16	1.83	0.007984	0.068324
WONG_EMBRYONIC_STEM_CELL_CORE	229	1.82	0.011538	0.076069
YAMASHITA_LIVER_CANCER_WITH_EPCAM_UP	37	1.81	0	0.079164
PID_HDAC_CLASSI_PATHWAY	45	1.81	0.016	0.079196
GRADE_COLON_CANCER_UP	489	1.80	0.00202	0.081345
REACTOME_FORMATION_OF_THE_HIV1_EARLY_ELONGATION_COMPLEX	22	1.80	0.014085	0.080019
REACTOME_RNA_POL_II_TRANSCRIPTION	64	1.80	0.014028	0.082773
REACTOME_PROCESSING_OF_CAPPED_INTRONLESS_PRE_MRNA	15	1.80	0.007968	0.081847
DAZARD_RESPONSE_TO_UV_SCC_DN	90	1.80	0.004049	0.082238
REACTOME_METABOLISM_OF_MRNA	132	1.79	0.027451	0.08535
LEE_LIVER_CANCER_SURVIVAL_DN	112	1.79	0.013487	0.084406
ABRAMSON_INTERACT_WITH_AIRE	33	1.79	0.013308	0.083706
REACTOME_RNA_POL_III_TRANSCRIPTION	26	1.79	0.020284	0.084122
REACTOME_RNA_POL_I_TRANSCRIPTION_INITIATION	17	1.78	0.019802	0.084954
REACTOME_PROTEIN_FOLDING	27	1.78	0.014028	0.088927
ZAMORA_NOS2_TARGETS_UP	45	1.77	0.023346	0.09044
REACTOME_REGULATORY_RNA_PATHWAYS	18	1.77	0.029821	0.092709
JAZAERI_BREAST_CANCER_BRCA1_VS_BRCA2_UP	32	1.77	0.010352	0.093477
COLLIS_PRKDC_SUBSTRATES	16	1.77	0.005952	0.094372
KEGG_RIBOSOME	43	1.76	0.024691	0.100544
SCHLOSSER_MYC_TARGETS_REPRESSED_BY_SERUM	108	1.75	0.041916	0.105971
REACTOME_NOTCH1_INTRACELLULAR_DOMAIN_REGULATES_TRANSCRIPTION	29	1.75	0.013752	0.104573
EPPERT_LSC_R	27	1.75	0.012346	0.107076
CHNG_MULTIPLE_MYELOMA_HYPERPLOID_UP	29	1.74	0.043764	0.107467
KYNG_WERNER_SYNDROM_AND_NORMAL_AGING_UP	57	1.74	0	0.108599
REACTOME_RECRUITMENT_OF_MITOTIC_CENTROSOME_PROTEINS_AND_COMPLEXES	38	1.73	0.01378	0.115908
REACTOME_TRANSPORT_OF_MATURE_TRANSCRIPT_TO_CYTOPLASM	34	1.73	0.028226	0.118997
REACTOME_MRNA_CAPPING	19	1.73	0.025692	0.118905
REACTOME_LOSS_OF_NLP_FROM_MITOTIC_CENTROSOMES	35	1.73	0.021401	0.118328
BIOCARTA_PYK2_PATHWAY	22	1.73	0.027944	0.120425
POMEROY_MEDULLOBLASTOMA_PROGNOSIS_DN	28	1.73	0.009921	0.118919
TOYOTA_TARGETS_OF_MIR34B_AND_MIR34C	225	1.72	0.011905	0.126031
MUELLER_PLURINET	202	1.72	0.017717	0.127631

SU_TESTIS	61	1.71	0.017341	0.12722
REACTOME_PEPTIDE_CHAIN_ELONGATION	42	1.71	0.020284	0.13039
LIN_MELANOMA_COPY_NUMBER_UP	44	1.70	0.006122	0.136901
VANHARANTA_UTERINE_FIBROID_WITH_7Q_DELETION_UP	52	1.70	0.017613	0.137154

NT-liver fibrosis HCCs

NAME	SIZE	NES	NOM p-val	FDR q-val
HOSHIDA_LIVER_CANCER_SURVIVAL_DN	90	2	0	0.1179
MOOTHA_HUMAN_MITODB_6_2002	327	1.99	0	0.0776
MOOTHA_MITOCHONDRIA	337	1.99	0	0.0555
KEGG_PEROXISOME	57	1.97	0	0.0544
KEGG_LYSINE_DEGRADATION	32	1.97	0	0.0442
ACEVEDO_NORMAL_TISSUE_ADJACENT_TO_LIVER_TUMOR_DN	211	1.96	0.004	0.0386
REACTOME_METABOLISM_OF_AMINO_ACIDS_AND_DERIVATIVES	137	1.95	0.002	0.0378
HOSHIDA_LIVER_CANCER_SUBCLASS_S3	217	1.91	0	0.0553
WOO_LIVER_CANCER_RECURRENCE_DN	61	1.90	0	0.0572
IIZUKA_LIVER_CANCER_PROGRESSION_G2_G3_UP	20	1.88	0	0.0608
LEE_LIVER_CANCER_SURVIVAL_UP	112	1.88	0	0.0611
BOYAULT_LIVER_CANCER_SUBCLASS_G1_DN	35	1.87	0	0.0614
REACTOME_PEROXISOMAL_LIPID_METABOLISM	15	1.83	0	0.0859
REACTOME_SULFUR_AMINO_ACID_METABOLISM	21	1.83	0.004	0.0837
LEE_LIVER_CANCER_DENA_DN	58	1.82	0	0.0828
GUO_TARGETS_OF_IRS1_AND_IRS2	70	1.81	0	0.0853
KEGG_VALINE_LEUCINE_AND_ISOLEUCINE_DEGRADATION	34	1.81	0.0077	0.0819
KEGG_PROPANOATE_METABOLISM	21	1.80	0.0039	0.0827
KEGG_HISTIDINE_METABOLISM	20	1.80	0.004	0.0863
KEGG_BETA_ALANINE_METABOLISM	18	1.79	0.0019	0.0837
KEGG_FATTY_ACID_METABOLISM	29	1.79	0	0.0849
REACTOME_RESPIRATORY_ELECTRON_TRANSPORT	40	1.78	0.0333	0.0898
LEE_LIVER_CANCER_ACOX1_DN	53	1.77	0.002	0.094
FLECHNER_BIOPSY_KIDNEY_TRANSPLANT_REJECTED_VS_OK_DN	411	1.77	0.004	0.0928
CHIANG_LIVER_CANCER_SUBCLASS_PROLIFERATION_DN	121	1.76	0	0.0928
BOYAULT_LIVER_CANCER_SUBCLASS_G123_DN	40	1.76	0	0.0907
LEE_LIVER_CANCER_CIPROFIBRATE_DN	51	1.76	0	0.0888
HSIAO_LIVER_SPECIFIC_GENES	193	1.76	0.0021	0.0859
OHGUCHI_LIVER_HNF4A_TARGETS_DN	81	1.76	0	0.0835
REACTOME_FATTY_ACID_TRIACYLGLYCEROL_AND_KETONE_BODY_METABOLISM	108	1.75	0.002	0.0847
LEE_LIVER_CANCER_MYC_TGFA_DN	54	1.75	0.004	0.0841
KEGG_GLYCINE_SERINE_AND_THREONINE_METABOLISM	25	1.75	0	0.0856
REACTOME_METABOLISM_OF_LIPIDS_AND_LIPOPROTEINS	304	1.75	0.0019	0.0837

BOCHKIS_FOXA2_TARGETS	265	1.74	0.0021	0.0838
KEGG_BUTANOATE_METABOLISM	27	1.74	0.0019	0.0818
WANG_CLASSIC_ADIPOGENIC_TARGETS_OF_PPARG	17	1.74	0.0019	0.0804
BOYAULT_LIVER_CANCER_SUBCLASS_G3_DN	39	1.74	0	0.0793
BOYAULT_LIVER_CANCER_SUBCLASS_G6_UP	51	1.74	0	0.0791
KEGG_TYROSINE_METABOLISM	25	1.73	0	0.0826
KEGG_TRYPTOPHAN_METABOLISM	27	1.72	0.002	0.09
KEGG_CYSTEINE_AND_METHIONINE_METABOLISM	24	1.72	0.004	0.0882
WONG_MITOCHONDRIA_GENE_MODULE	145	1.72	0.0413	0.0875
MOOTHA_GLYCOGEN_METABOLISM	15	1.71	0.002	0.0906
LUCAS_HNF4A_TARGETS_UP	44	1.71	0.0119	0.0915

Supplementary Table 7. ***Bibliographical summary of the 27 proteins from the fibrous nest signature.***

Gene symbol	Known role in cancer[a]	Known role in HCC progression[b]	Known role in liver carcinogenesis[c]	Reference	Known mechanism of action
COL1A1	Yes	Yes	Yes	(23, 24)	Type I collagen promotes proliferation and tumour development through increased stiffness and activation of TAZ in pretumoural hepatocytes and discoidin domain receptor 1 in established tumours.
COL1A2	Yes	Yes	Yes		
COL3A1	Yes	No	No	(25, 26)	Integrin-mediated activation of NFκB and potential role in PD-L1 expression
COL4A1	Yes	Yes	No	(27, 28)	FAK-Src signaling
COL4A2	Yes	No	No	(29)	
COL5A1	Yes	No	No	(30, 31)	TGF-β signaling; stabilizes collagen-type I supramolecular assemblies.
COL5A2	Yes	No	No	(32, 33)	WNT/β-catenin and PI3K/mTOR signaling
COL10A1	Yes	No	No	(34, 35)	TGF-β/Smad signaling, FAK-Src signaling
COL16A1	Yes	No	No	(36)	Integrin activation
COMP	Yes	Yes	No	(37)	CD36 mediated activation of MEK signaling + PI3K/Akt, Integrin mediated activation of Src signaling, Notch 3 signaling
EFEMP1	Yes	Yes	No	(38, 39)	Activation of EGFR signaling. Putative tumor suppressor role in HCC by regulating ERK signaling.
FBN1	Yes	No	No	(40, 41)	VEGFR2 signaling
IGFBP7	Yes	Yes	No	(42, 43)	TGF-β/Smad signaling, CD93 ligand. Putative tumor suppressor role in HCC by activation of IGF1 receptor
LAMB1	Yes	Yes	No	(44)	PDGFR-KRT19 signaling
LAMC1	Yes	Yes	No	(45)	NFκB-CXCL1-STAT3 signaling
LTBP2	Yes	No	No	(46, 47)	NFκB signaling
MFAP2	Yes	Yes	No	(48, 49)	FOXM1 and Wnt/β-catenin signaling
POSTN	Yes	Yes	Yes	(50, 51)	Pi3K/Akt signaling, NFκB signaling
TNC	Yes	No	No	(52)	Wnt and MAPK signaling, YAP signaling.
HSPG2	Yes	No	No	(53, 54)	VEGF signaling
LUM	Yes	Yes	Yes	(55)	IGF-IR, ERK-1, and JNK signaling
VCAN	Yes	Yes	No	(56)	EGFR-PI3K-AKT signaling
LOX	Yes	Yes	Yes	(57, 58)	Collagen crosslinking, thereby increasing matrix stiffness and subsequent integrin signaling
ANXA1	Yes	No	No	(59)	TGF-β signaling
LGALS1	Yes	Yes	No	(60)	Pi3K/Akt signaling
LGALS3	Yes	Yes	No	(61)	β-catenin signaling
CXCL13	Yes	Yes	No	(62, 63)	Association with T-cell exhaustion

a: evidence of a role on cancer cell proliferation, stemness or migration based on in vitro assay.
b: evidence of a role on HCC proliferation, stemness or migration based on in vitro assay.
c: evidence of a role on HCC initiation based on in vivo model of carcinogenesis.

Supplementary Table 8. ***List of antibodies***

Name	Company	Species	Reference	Clone
VCAN-CF488	Clinisciences	Rb	ORB13754-CF488A-	poly
ANXA1-DL680	Biotechne	Ms	NBP2-70174FR	OTI3A8
FBN1-A750	Clinisciences	Rb	BS-1157R-A750	Poly
CXCL13-Y2	Novusbio	Rb	NBP2-16041G	Poly
ADAM10-Y3	Biotechne	Ms	NBP2-12014R	MM0077-6D31
POSTN-Y7	Clinisciences	Ms	SC-398631 AF790	F-10
ANXA5-Y2	Biotechne	Ms	NB100-63307	VAA-33
COL5A1-Y3	Novusbio	Ms	NBP1-05118R	1E2-E4/Col5
DPT-Y5	Santa cruz	MS	sc-376863 AF680	F-4
ELN-Y7	Biotechne	Ms	NBP3-08889IR	ELN/2069
COL1A1-Y2	Biotechne	Rb	NBP1-77457G	Poly
CD45-Y3	Biotechne	Rb	NBP3-08910R	PTPRC/1975R
ACTA2-Y5	Biotechne	Ms	NBP2-34522FR	1A4/asm-1
CD31-Y3	Abcam	Rb	ab279331	EPR309
HK2	Proteintech	Rb	22029-1-AP	Poly

BIBLIOGRAPHY

1. Lee JS, Chu IS, Mikaelyan A, Calvisi DF, Heo J, Reddy JK, Thorgeirsson SS. Application of comparative functional genomics to identify best-fit mouse models to study human cancer. Nat Genet 2004;36:1306-1311.

2. Chen B, Liu L, Castonguay A, Maronpot RR, Anderson MW, You M. Dose-dependent ras mutation spectra in N-nitrosodiethylamine induced mouse liver tumors and 4-(methylnitrosamino)-1-(3-pyridyl)-1-butanone induced mouse lung tumors. Carcinogenesis 1993;14:1603-1608.

3. Kall L, Storey JD, Noble WS. Non-parametric estimation of posterior error probabilities associated with peptides identified by tandem mass spectrometry. Bioinformatics 2008;24:i42-48.

4. Nesvizhskii AI, Keller A, Kolker E, Aebersold R. A statistical model for identifying proteins by tandem mass spectrometry. Anal Chem 2003;75:4646-4658.

5. Desert R, Rohart F, Canal F, Sicard M, Desille M, Renaud S, Turlin B, et al. Human hepatocellular carcinomas with a periportal phenotype have the lowest potential for early recurrence after curative resection. Hepatology 2017;66:1502-1518.

6. Johnson WE, Li C, Rabinovic A. Adjusting batch effects in microarray expression data using empirical Bayes methods. Biostatistics 2007;8:118-127.

7. Hynes RO, Naba A. Overview of the matrisome--an inventory of extracellular matrix constituents and functions. Cold Spring Harb Perspect Biol 2012;4:a004903.

8. Naba A, Clauser KR, Hoersch S, Liu H, Carr SA, Hynes RO. The matrisome: in silico definition and in vivo characterization by proteomics of normal and tumor extracellular matrices. Mol Cell Proteomics 2012;11:M111 014647.

9. Naba A, Hoersch S, Hynes RO. Towards definition of an ECM parts list: an advance on GO categories. Matrix Biol 2012;31:371-372.

10. Subramanian A, Tamayo P, Mootha VK, Mukherjee S, Ebert BL, Gillette MA, Paulovich A, et al. Gene set enrichment analysis: a knowledge-based approach for interpreting genome-wide expression profiles. Proc Natl Acad Sci U S A 2005;102:15545-15550.

11. Shannon P, Markiel A, Ozier O, Baliga NS, Wang JT, Ramage D, Amin N, et al. Cytoscape: a software environment for integrated models of biomolecular interaction networks. Genome Res 2003;13:2498-2504.

12. Kim H, Choi GH, Na DC, Ahn EY, Kim GI, Lee JE, Cho JY, et al. Human hepatocellular carcinomas with "Stemness"-related marker expression: keratin 19 expression and a poor prognosis. Hepatology 2011;54:1707-1717.

13. Yamashita T, Ji J, Budhu A, Forgues M, Yang W, Wang HY, Jia H, et al. EpCAM-positive hepatocellular carcinoma cells are tumor-initiating cells with stem/progenitor cell features. Gastroenterology 2009;136:1012-1024.

14. Guo X, Xiong L, Sun T, Peng R, Zou L, Zhu H, Zhang J, et al. Expression features of SOX9 associate with tumor progression and poor prognosis of hepatocellular carcinoma. Diagn Pathol 2012;7:44.

15. Huang da W, Sherman BT, Lempicki RA. Systematic and integrative analysis of large gene lists using DAVID bioinformatics resources. Nat Protoc 2009;4:44-57.

16. Roy S, Hooiveld GJ, Seehawer M, Caruso S, Heinzmann F, Schneider AT, Frank AK, et al. microRNA 193a-5p Regulates Levels of Nucleolar- and Spindle-Associated Protein 1 to Suppress Hepatocarcinogenesis. Gastroenterology 2018;155:1951-1966 e1926.

17. Mebarki S, Desert R, Sulpice L, Sicard M, Desille M, Canal F, Dubois-Pot Schneider H, et al. De novo HAPLN1 expression hallmarks Wnt-induced stem cell and fibrogenic networks leading to aggressive human hepatocellular carcinomas. Oncotarget 2016;7:39026-39043.

18. Sung WK, Zheng H, Li S, Chen R, Liu X, Li Y, Lee NP, et al. Genome-wide survey of recurrent HBV integration in hepatocellular carcinoma. Nat Genet 2012;44:765-769.

19. Roessler S, Jia HL, Budhu A, Forgues M, Ye QH, Lee JS, Thorgeirsson SS, et al. A unique metastasis gene signature enables prediction of tumor relapse in early-stage hepatocellular carcinoma patients. Cancer Res 2010;70:10202-10212.

20. Hoshida Y, Villanueva A, Kobayashi M, Peix J, Chiang DY, Camargo A, Gupta S, et al. Gene expression in fixed tissues and outcome in hepatocellular carcinoma. N Engl J Med 2008;359:1995-2004.

21. Tsuchiya M, Parker JS, Kono H, Matsuda M, Fujii H, Rusyn I. Gene expression in nontumoral liver tissue and recurrence-free survival in hepatitis C virus-positive hepatocellular carcinoma. Mol Cancer 2010;9:74.

22. Cancer Genome Atlas Research Network. Electronic address wbe, Cancer Genome Atlas Research N. Comprehensive and Integrative Genomic Characterization of Hepatocellular Carcinoma. Cell 2017;169:1327-1341 e1323.

23. Fujisaki H, Futaki S. Epithelial-Mesenchymal Transition Induced in Cancer Cells by Adhesion to Type I Collagen. Int J Mol Sci 2022;24.

24. Filliol A, Saito Y, Nair A, Dapito DH, Yu LX, Ravichandra A, Bhattacharjee S, et al. Opposing roles of hepatic stellate cell subpopulations in hepatocarcinogenesis. Nature 2022;610:356-365.

25. Yang F, Lin L, Li X, Wen R, Zhang X. Silencing of COL3A1 represses proliferation, migration, invasion, and immune escape of triple negative breast cancer cells via down-regulating PD-L1 expression. Cell Biol Int 2022;46:1959-1969.

26. Zhou J, Yang Y, Zhang H, Luan S, Xiao X, Li X, Fang P, et al. Overexpressed COL3A1 has prognostic value in human esophageal squamous cell carcinoma and promotes the aggressiveness of esophageal squamous cell carcinoma by activating the NF-kappaB pathway. Biochem Biophys Res Commun 2022;613:193-200.

27. Zhang H, Wang Y, Ding H. COL4A1, negatively regulated by XPD and miR-29a-3p, promotes cell proliferation, migration, invasion and epithelial-mesenchymal transition in liver cancer cells. Clin Transl Oncol 2021;23:2078-2089.

28. Wang T, Jin H, Hu J, Li X, Ruan H, Xu H, Wei L, et al. COL4A1 promotes the growth and metastasis of hepatocellular carcinoma cells by activating FAK-Src signaling. J Exp Clin Cancer Res 2020;39:148.

29. JingSong H, Hong G, Yang J, Duo Z, Li F, WeiCai C, XueYing L, et al. siRNA-mediated suppression of collagen type iv alpha 2 (COL4A2) mRNA inhibits triple-negative breast cancer cell proliferation and migration. Oncotarget 2017;8:2585-2593.

30. Yang M, Lu Z, Yu B, Zhao J, Li L, Zhu K, Ma M, et al. COL5A1 Promotes the Progression of Gastric Cancer by Acting as a ceRNA of miR-137-3p to Upregulate FSTL1 Expression. Cancers (Basel) 2022;14.

31. Park Y, Park M, Kim J, Ahn J, Sim J, Bang JI, Heo J, et al. NOX2-Induced High Glycolytic Activity Contributes to the Gain of COL5A1-Mediated Mesenchymal Phenotype in GBM. Cancers (Basel) 2022;14.

32. Ren X, Chen X, Fang K, Zhang X, Wei X, Zhang T, Li G, et al. COL5A2 Promotes Proliferation and Invasion in Prostate Cancer and Is One of Seven Gleason-Related Genes That Predict Recurrence-Free Survival. Front Oncol 2021;11:583083.

33. Wang J, Jiang YH, Yang PY, Liu F. Increased Collagen Type V alpha2 (COL5A2) in Colorectal Cancer is Associated with Poor Prognosis and Tumor Progression. Onco Targets Ther 2021;14:2991-3002.

34. Kahlert UD, Shi W, Strecker M, Scherpinski LA, Wartmann T, Dolling M, Perrakis A, et al. COL10A1 allows stratification of invasiveness of colon cancer and associates to extracellular matrix and immune cell enrichment in the tumor parenchyma. Front Oncol 2022;12:1007514.

35. Sun Y, Ling J, Liu L. Collagen type X alpha 1 promotes proliferation, invasion and epithelial-mesenchymal transition of cervical cancer through activation of TGF-beta/Smad signaling. Physiol Int 2022.

36. Grassel S, Bauer RJ. Collagen XVI in health and disease. Matrix Biol 2013;32:64-73.

37. Li Q, Wang C, Wang Y, Sun L, Liu Z, Wang L, Song T, et al. HSCs-derived COMP drives hepatocellular carcinoma progression by activating MEK/ERK and PI3K/AKT signaling pathways. J Exp Clin Cancer Res 2018;37:231.

38. Hu J, Duan B, Jiang W, Fu S, Gao H, Lu L. Epidermal growth factor-containing fibulin-like extracellular matrix protein 1 (EFEMP1) suppressed the growth of hepatocellular carcinoma cells by promoting Semaphorin 3B(SEMA3B). Cancer Med 2019;8:3152-3166.

39. Dou CY, Cao CJ, Wang Z, Zhang RH, Huang LL, Lian JY, Xie WL, et al. EFEMP1 inhibits migration of hepatocellular carcinoma by regulating MMP2 and MMP9 via ERK1/2 activity. Oncol Rep 2016;35:3489-3495.

40. Wang Z, Chen W, Zuo L, Xu M, Wu Y, Huang J, Zhang X, et al. The Fibrillin-1/VEGFR2/STAT2 signaling axis promotes chemoresistance via modulating glycolysis and angiogenesis in ovarian cancer organoids and cells. Cancer Commun (Lond) 2022;42:245-265.

41. Kerslake R, Hall M, Vagnarelli P, Jeyaneethi J, Randeva HS, Pados G, Kyrou I, et al. A pancancer overview of FBN1, asprosin and its cognate receptor OR4M1 with detailed expression profiling in ovarian cancer. Oncol Lett 2021;22:650.

42. Akiel M, Guo C, Li X, Rajasekaran D, Mendoza RG, Robertson CL, Jariwala N, et al. IGFBP7 Deletion Promotes Hepatocellular Carcinoma. Cancer Res 2017;77:4014-4025.

43. Yi X, Zheng X, Xu H, Li J, Zhang T, Ge P, Liao D, et al. IGFBP7 and the Tumor Immune Landscape: A Novel Target for Immunotherapy in Bladder Cancer. Front Immunol 2022;13:898493.

44. Liu T, Gan H, He S, Deng J, Hu X, Li L, Cai L, et al. RNA Helicase DDX24 Stabilizes LAMB1 to Promote Hepatocellular Carcinoma Progression. Cancer Res 2022;82:3074-3087.

45. Lee H, Kim WJ, Kang HG, Jang JH, Choi IJ, Chun KH, Kim SJ. Upregulation of LAMB1 via ERK/c-Jun Axis Promotes Gastric Cancer Growth and Motility. Int J Mol Sci 2021;22.

46. Wang J, Jiang C, Li N, Wang F, Xu Y, Shen Z, Yang L, et al. The circEPSTI1/mir-942-5p/LTBP2 axis regulates the progression of OSCC in the background of OSF via EMT and the PI3K/Akt/mTOR pathway. Cell Death Dis 2020;11:682.

47. Wang J, Liang WJ, Min GT, Wang HP, Chen W, Yao N. LTBP2 promotes the migration and invasion of gastric cancer cells and predicts poor outcome of patients with gastric cancer. Int J Oncol 2018;52:1886-1898.

48. Zhu X, Cheng Y, Wu F, Sun H, Zheng W, Jiang W, Shi J, et al. MFAP2 Promotes the Proliferation of Cancer Cells and Is Associated With a Poor Prognosis in Hepatocellular Carcinoma. Technol Cancer Res Treat 2020;19:1533033820977524.

49. Zhao LQ, Sun W, Zhang P, Gao W, Fang CY, Zheng AW. MFAP2 aggravates tumor progression through activating FOXM1/beta-catenin-mediated glycolysis in ovarian cancer. Kaohsiung J Med Sci 2022;38:772-780.

50. Xiao H, Zhang Y, Li Z, Liu B, Cui D, Liu F, Chen D, et al. Periostin deficiency reduces diethylnitrosamine-induced liver cancer in mice by decreasing hepatic stellate cell activation and cancer cell proliferation. J Pathol 2021;255:212-223.

51. Jia Y, Zhong F, Jiang S, Guo Q, Jin H, Wang F, Li M, et al. Periostin in chronic liver diseases: Current research and future perspectives. Life Sci 2019;226:91-97.

52. Yilmaz A, Loustau T, Salome N, Poilil Surendran S, Li C, Tucker RP, Izzi V, et al. Advances on the roles of tenascin-C in cancer. J Cell Sci 2022;135.

53. Bonche R, Smolen P, Chessel A, Boisivon S, Pisano S, Voigt A, Schaub S, et al. Regulation of the collagen IV network by the basement membrane protein perlecan is crucial for squamous epithelial cell morphogenesis and organ architecture. Matrix Biol 2022;114:35-66.

54. Zhang W, Lin Z, Shi F, Wang Q, Kong Y, Ren Y, Lyu J, et al. HSPG2 Mutation Association with Immune Checkpoint Inhibitor Outcome in Melanoma and Non-Small Cell Lung Cancer. Cancers (Basel) 2022;14.

55. Giatagana EM, Berdiaki A, Tsatsakis A, Tzanakakis GN, Nikitovic D. Lumican in Carcinogenesis-Revisited. Biomolecules 2021;11.

56. Zhangyuan G, Wang F, Zhang H, Jiang R, Tao X, Yu D, Jin K, et al. VersicanV1 promotes proliferation and metastasis of hepatocellular carcinoma through the activation of EGFR-PI3K-AKT pathway. Oncogene 2020;39:1213-1230.

57. Zhao W, Lv M, Yang X, Zhou J, Xing B, Zhang Z. Liver tumor-initiating cells initiate the formation of a stiff cancer stem cell microenvironment niche by secreting LOX. Carcinogenesis 2022;43:766-778.

58. Lin HY, Li CJ, Yang YL, Huang YH, Hsiau YT, Chu PY. Roles of Lysyl Oxidase Family Members in the Tumor Microenvironment and Progression of Liver Cancer. Int J Mol Sci 2020;21.

59. Zheng L, Li L, Wang B, Zhang S, Fu Z, Cheng A, Liang X. Annexin A1 affects tumor metastasis through epithelial-mesenchymal transition: a narrative review. Transl Cancer Res 2022;11:4416-4433.

60. Tsai YT, Li CY, Huang YH, Chang TS, Lin CY, Chuang CH, Wang CY, et al. Galectin-1 orchestrates an inflammatory tumor-stroma crosstalk in hepatoma by enhancing TNFR1 protein stability and signaling in carcinoma-associated fibroblasts. Oncogene 2022;41:3011-3023.

61. An Y, Xu S, Liu Y, Xu X, Philips CA, Chen J, Mendez-Sanchez N, et al. Role of Galectins in the Liver Diseases: A Systematic Review and Meta-Analysis. Front Med (Lausanne) 2021;8:744518.

62. Wu SY, Liao P, Yan LY, Zhao QY, Xie ZY, Dong J, Sun HT. Correlation of MKI67 with prognosis, immune infiltration, and T cell exhaustion in hepatocellular carcinoma. BMC Gastroenterol 2021;21:416.

63. Zheng C, Fass JN, Shih YP, Gunderson AJ, Sanjuan Silva N, Huang H, Bernard BM, et al. Transcriptomic profiles of neoantigen-reactive T cells in human gastrointestinal cancers. Cancer Cell 2022;40:410-423 e417.

Supplementary Figure 1

A

Method: compartmental extraction kit
Sample: 1 liver fibrosis from CCl_4 treated mouse. Tissue weight: 118 mg

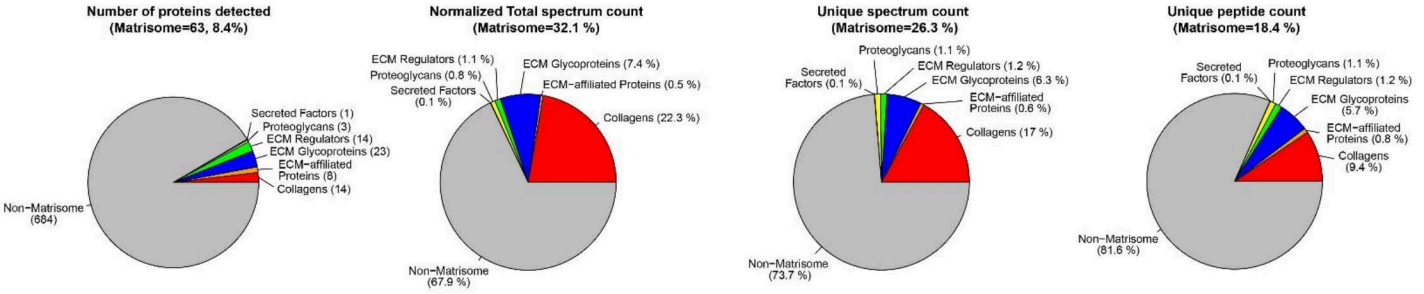

B

Method: compartmental extraction kit
Sample: 2 liver fibrosis from CCl_4 treated mouse. Tissue weight: 150 and 124 mg

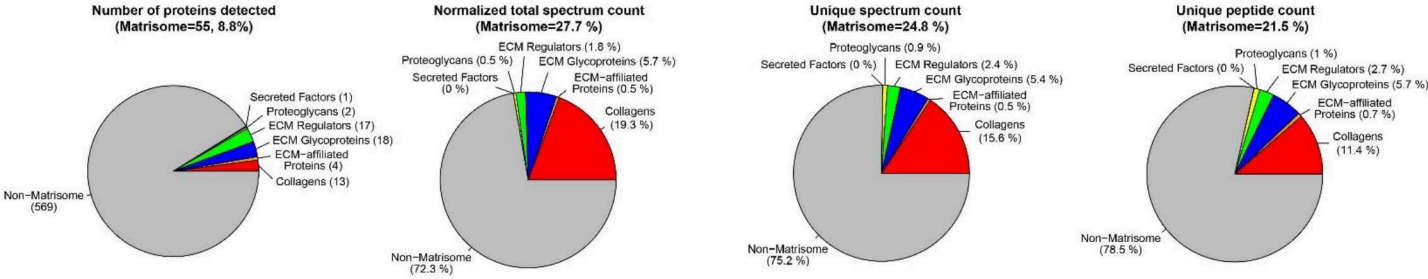

C

Method: decellularization
Sample: 1 human HCC in duplicate. Tissue weight: 50 and 30 mg

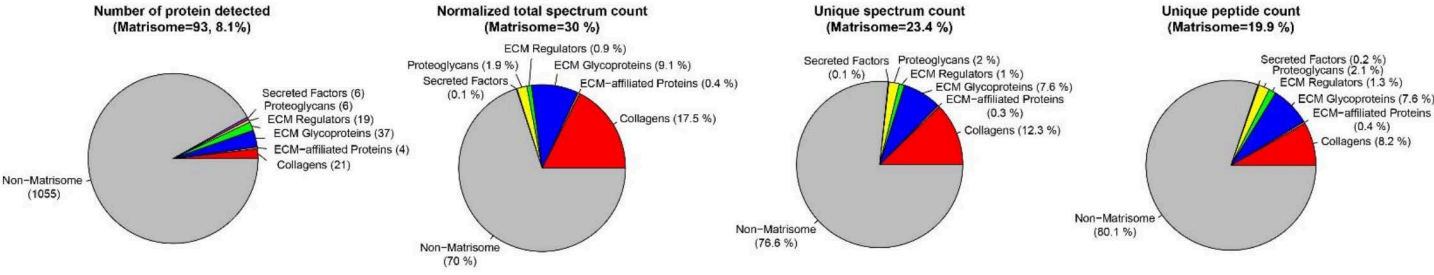

D

Method: decellularization
Sample: 2 human HCCs in duplicate. Tissue weight: 58, 66, 123 and 185 mg

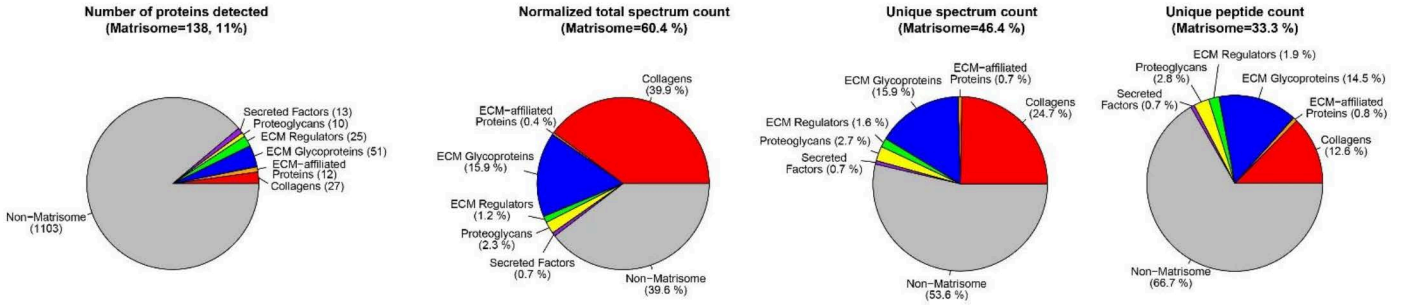

Supplementary Figure 1

E

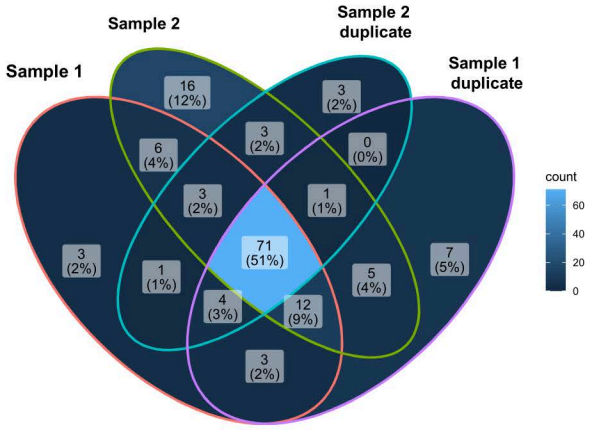

F

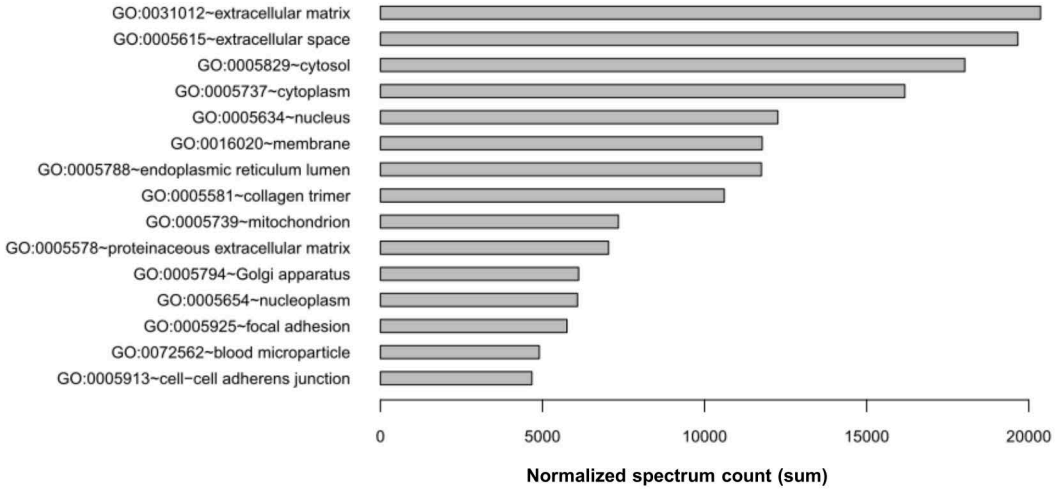

Supplementary Figure 2

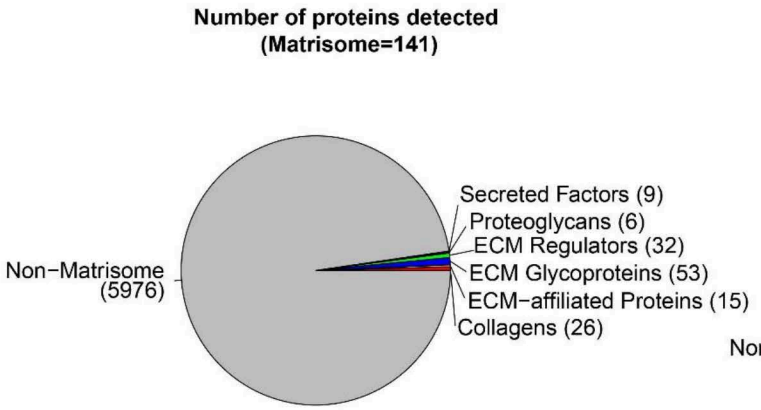

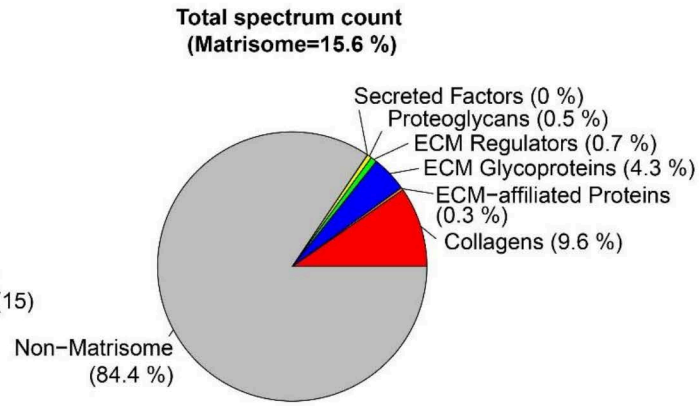

Supplementary Figure 3

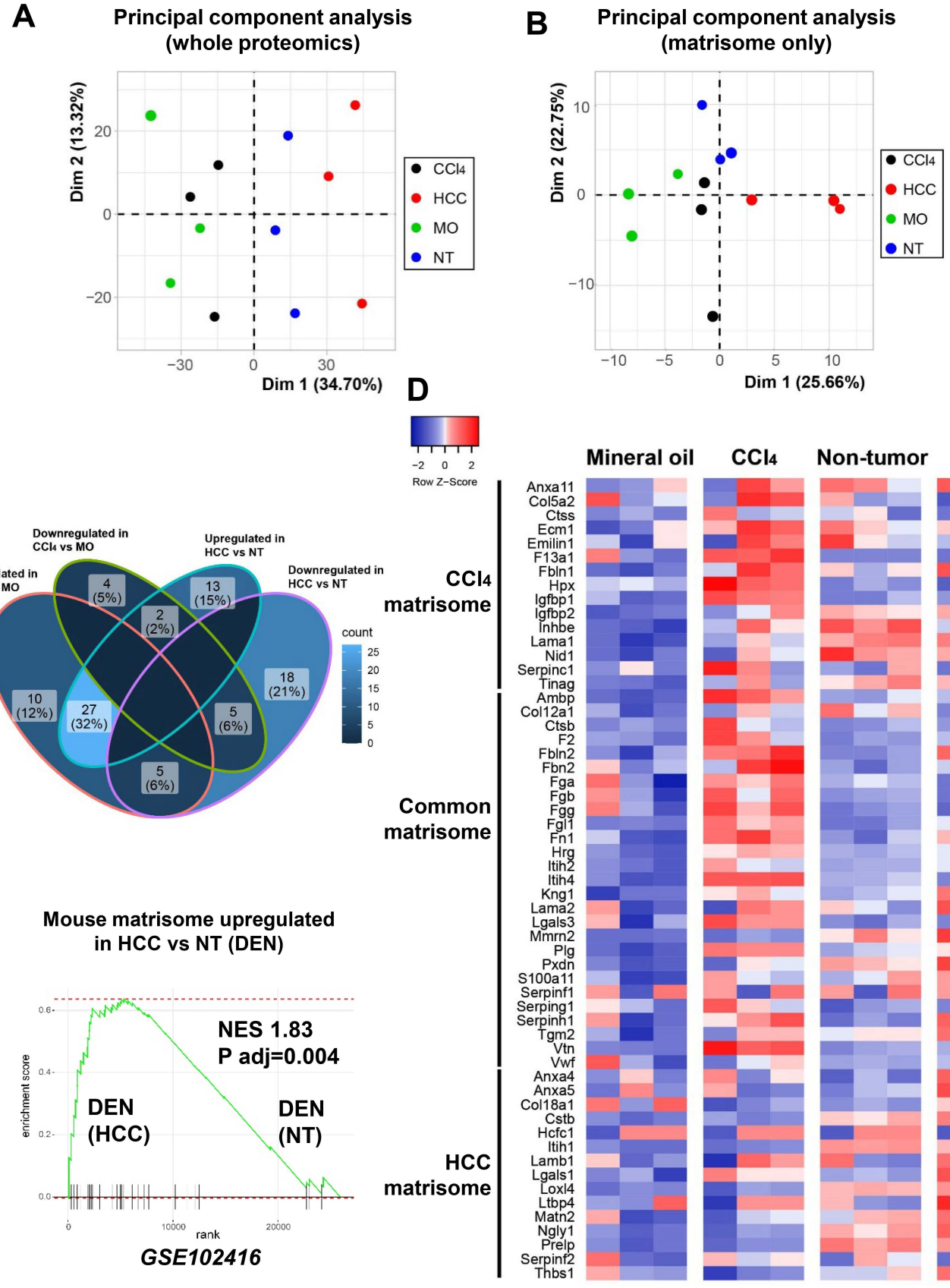

Supplementary Figure 4

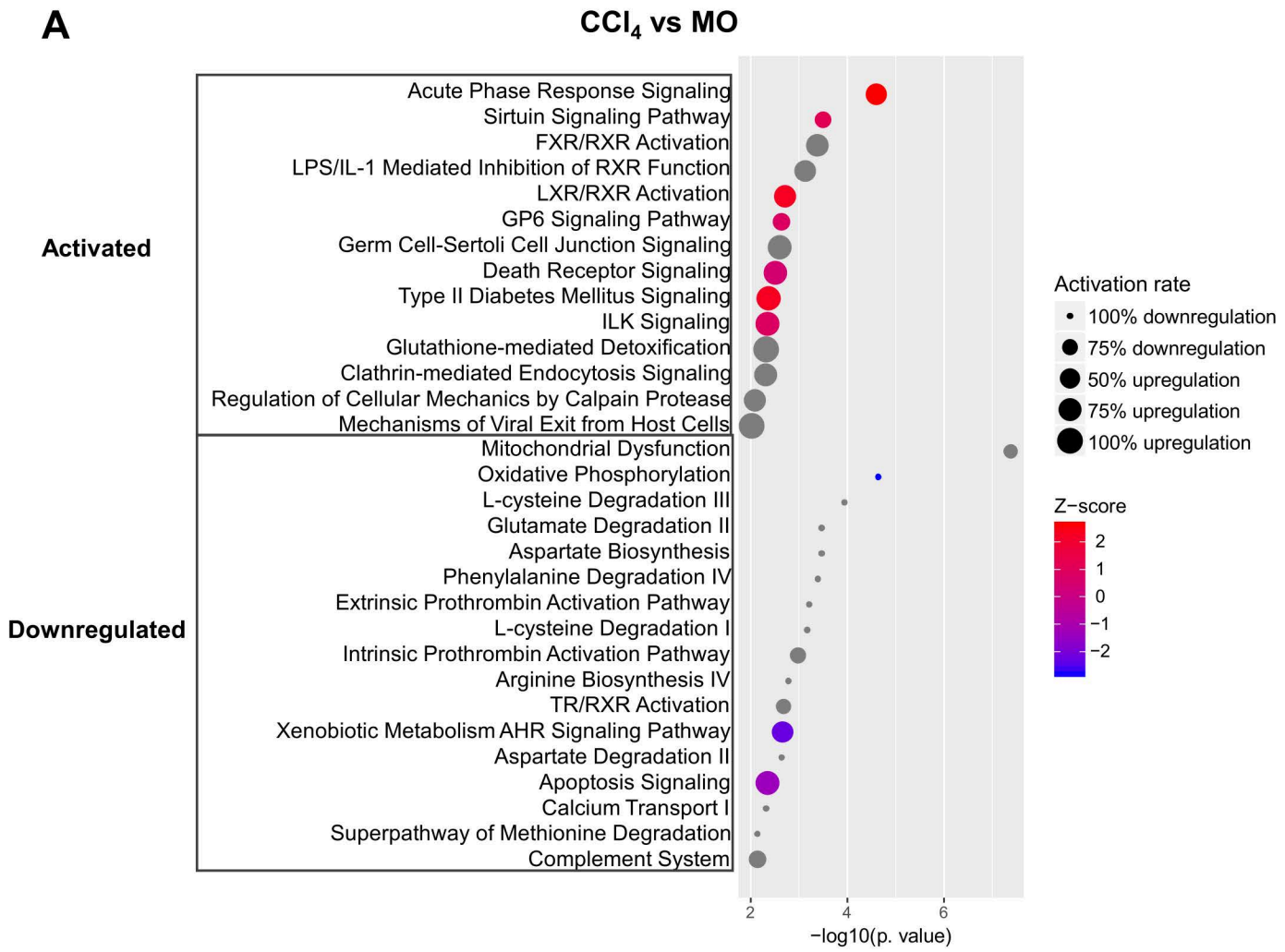

Supplementary Figure 4

B

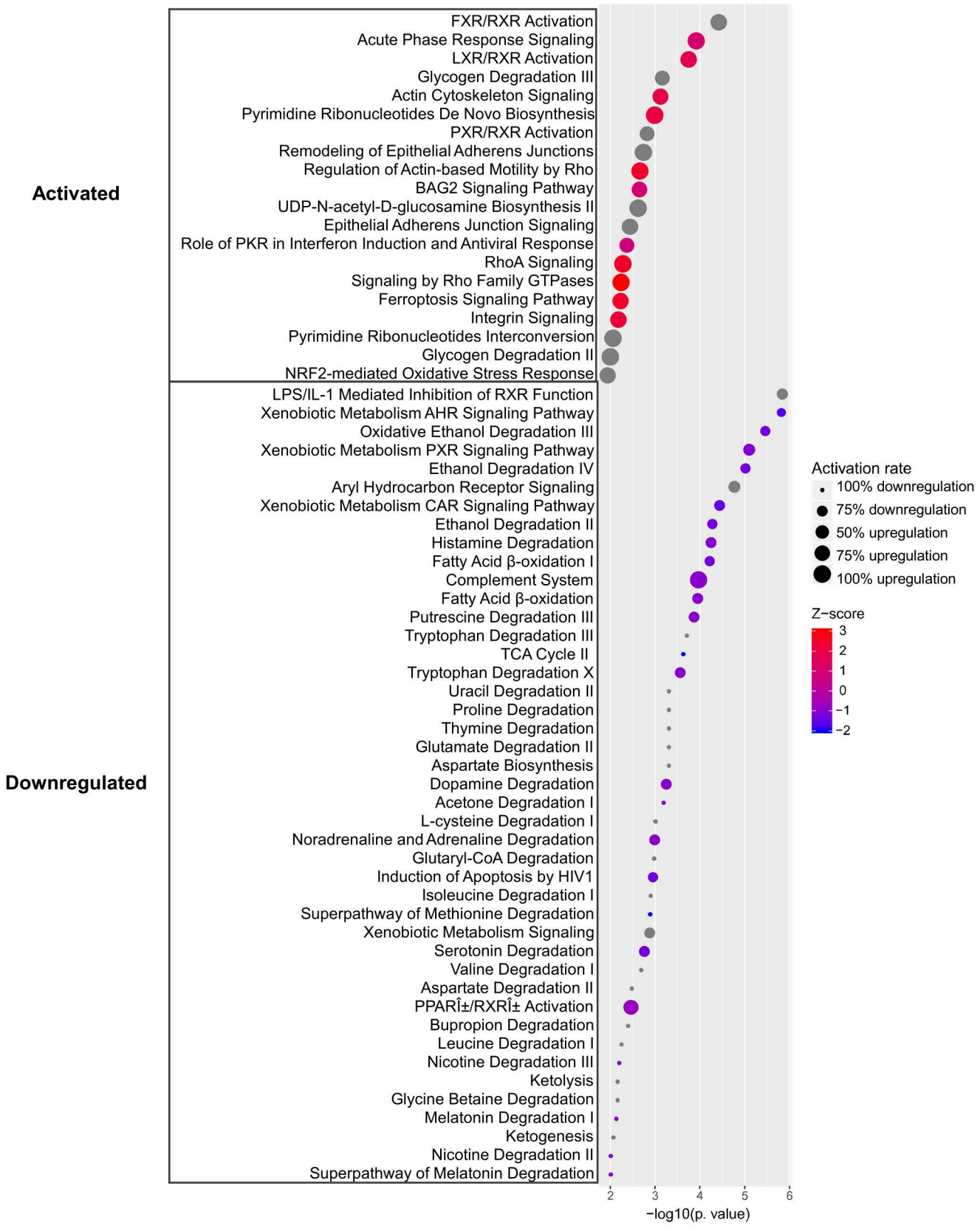

Supplementary Figure 4

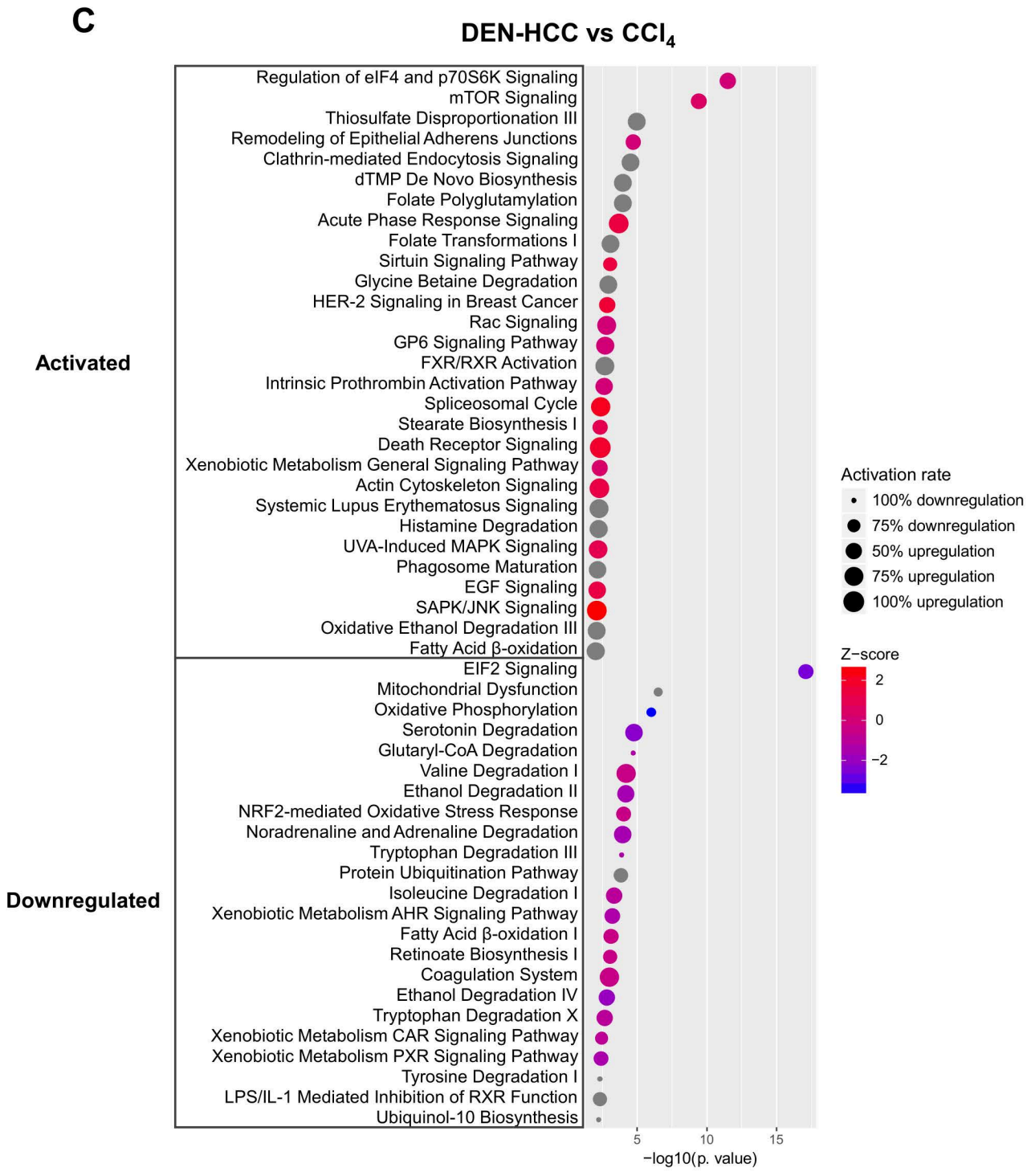

Supplementary Figure 5

Among the 42 proteins upregulated in DEN-induced HCC

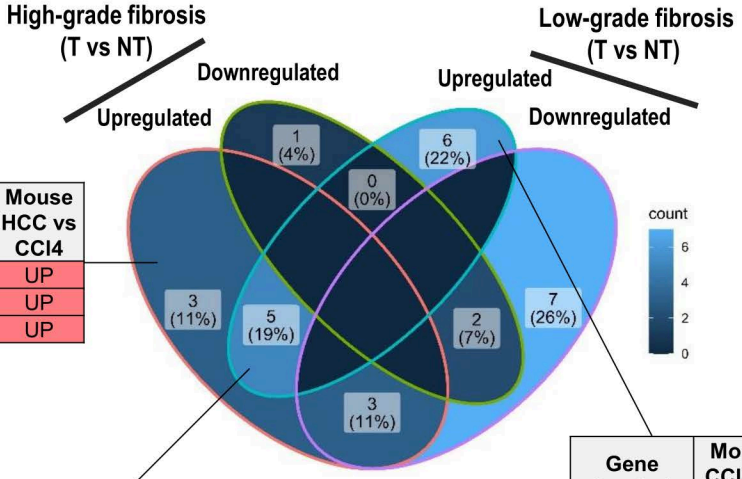

Gene Symbol	Mouse CCl4 vs MO	Mouse HCC vs NT	Mouse HCC vs CCl4
Lamb1	NS	UP	UP
Pxdn	UP	UP	UP
Vwf	UP	UP	UP

Gene Symbol	Mouse CCl4 vs MO	Mouse HCC vs NT	Mouse HCC vs CCl4
Col18a1	DN	UP	UP
Fga	UP	UP	NS
Fgb	UP	UP	NS
Fgg	UP	UP	DN
Fn1	UP	UP	NS

Gene Symbol	Mouse CCl4 vs MO	Mouse HCC vs NT	Mouse HCC vs CCl4
F2	UP	UP	NS
Itih2	UP	UP	UP
Kng1	UP	UP	UP
Plg	UP	UP	NS
Serpinh1	UP	UP	UP
Hcfc1	NS	UP	UP

Supplementary Figure 6

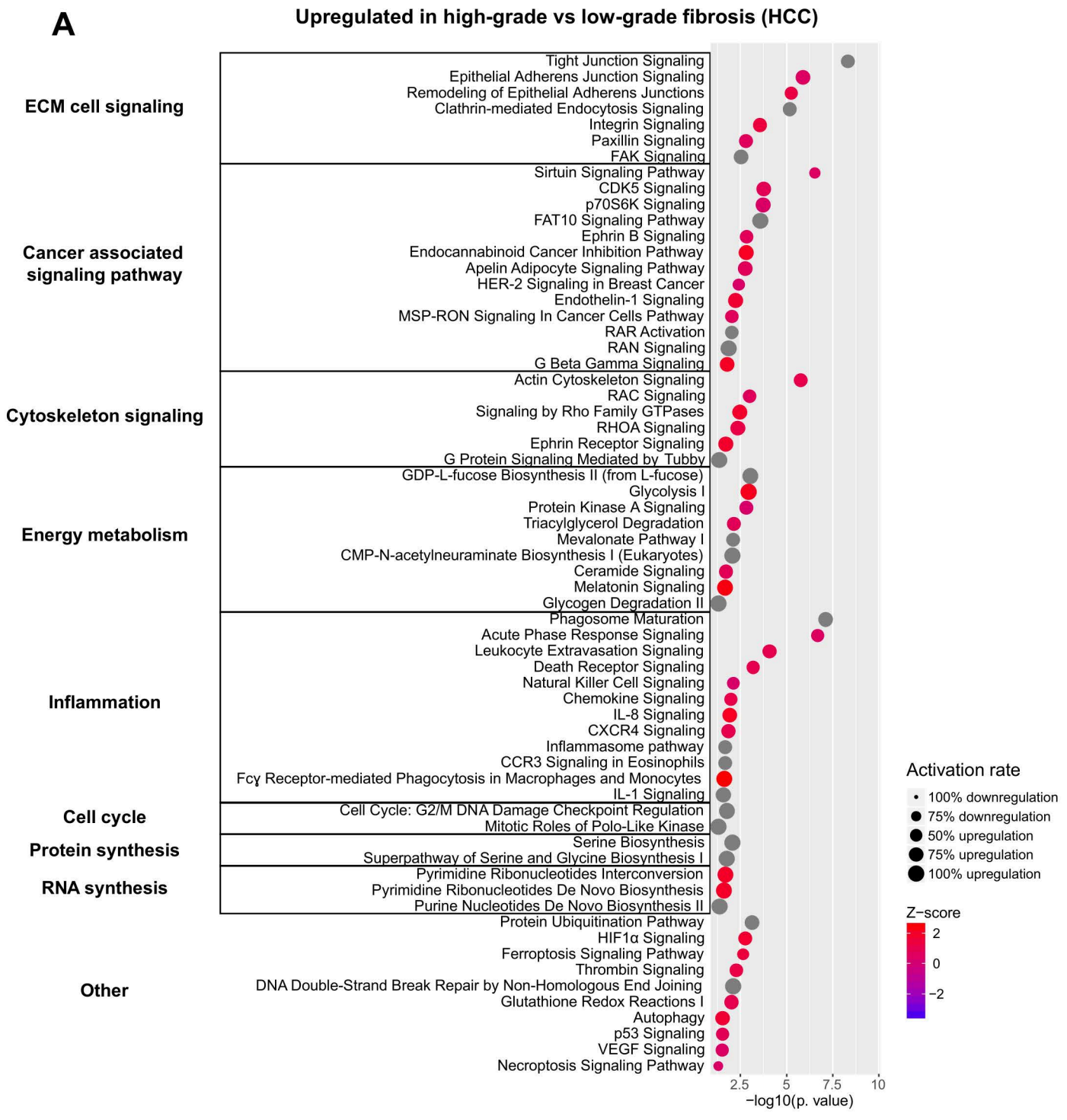

Supplementary Figure 6

B

Supplementary Figure 6

C

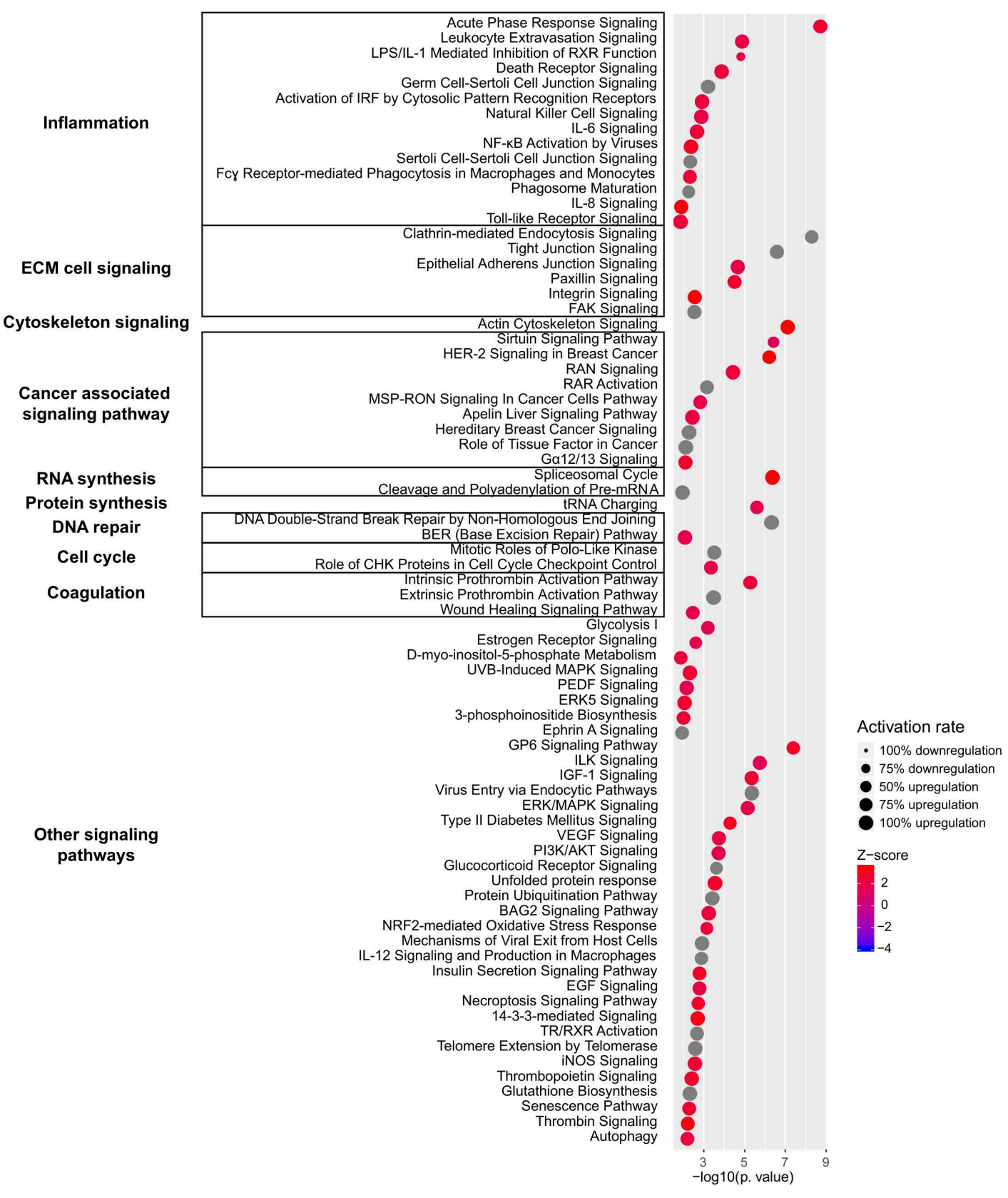

Supplementary Figure 6

D

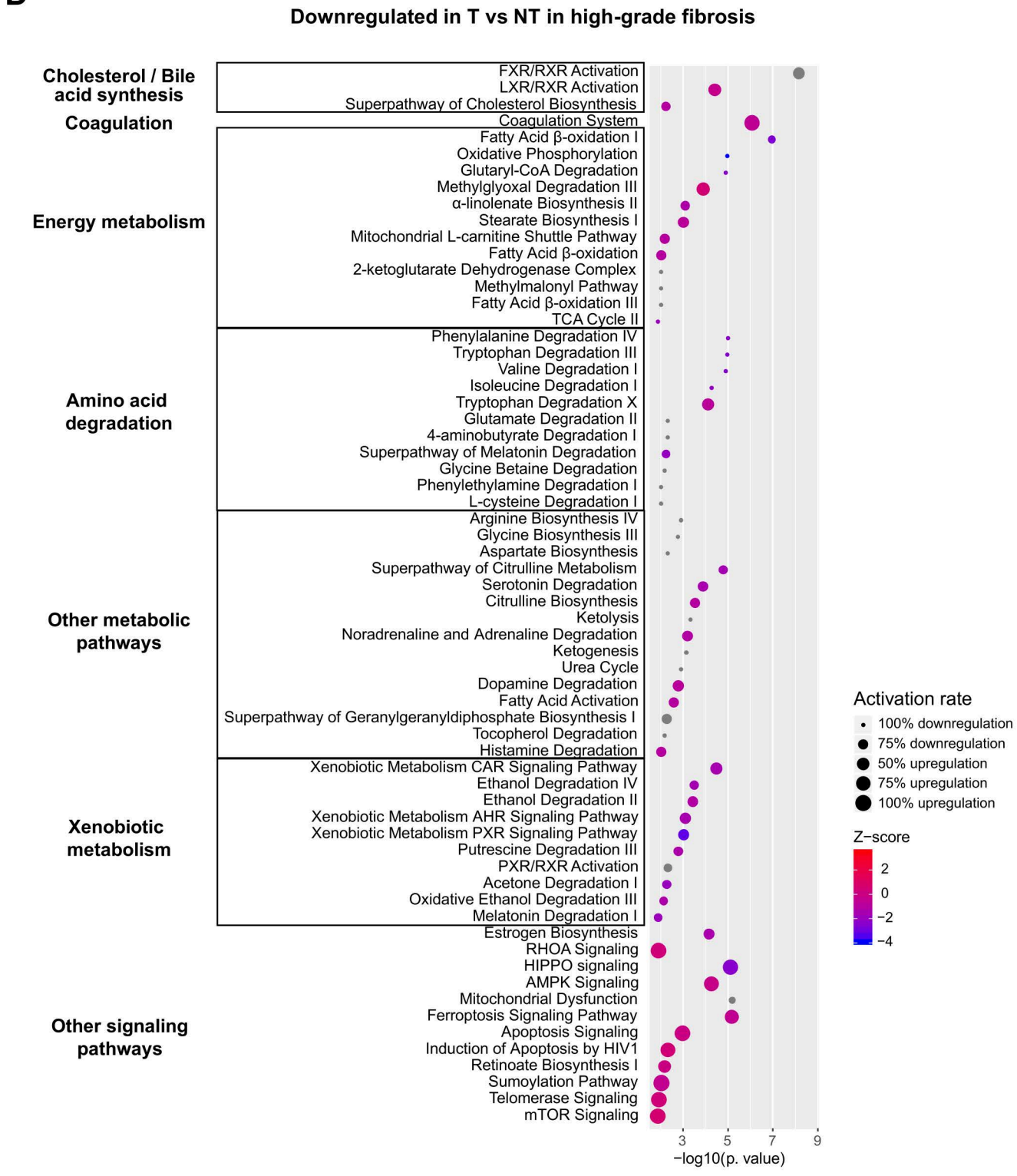

Supplementary Figure 6

E

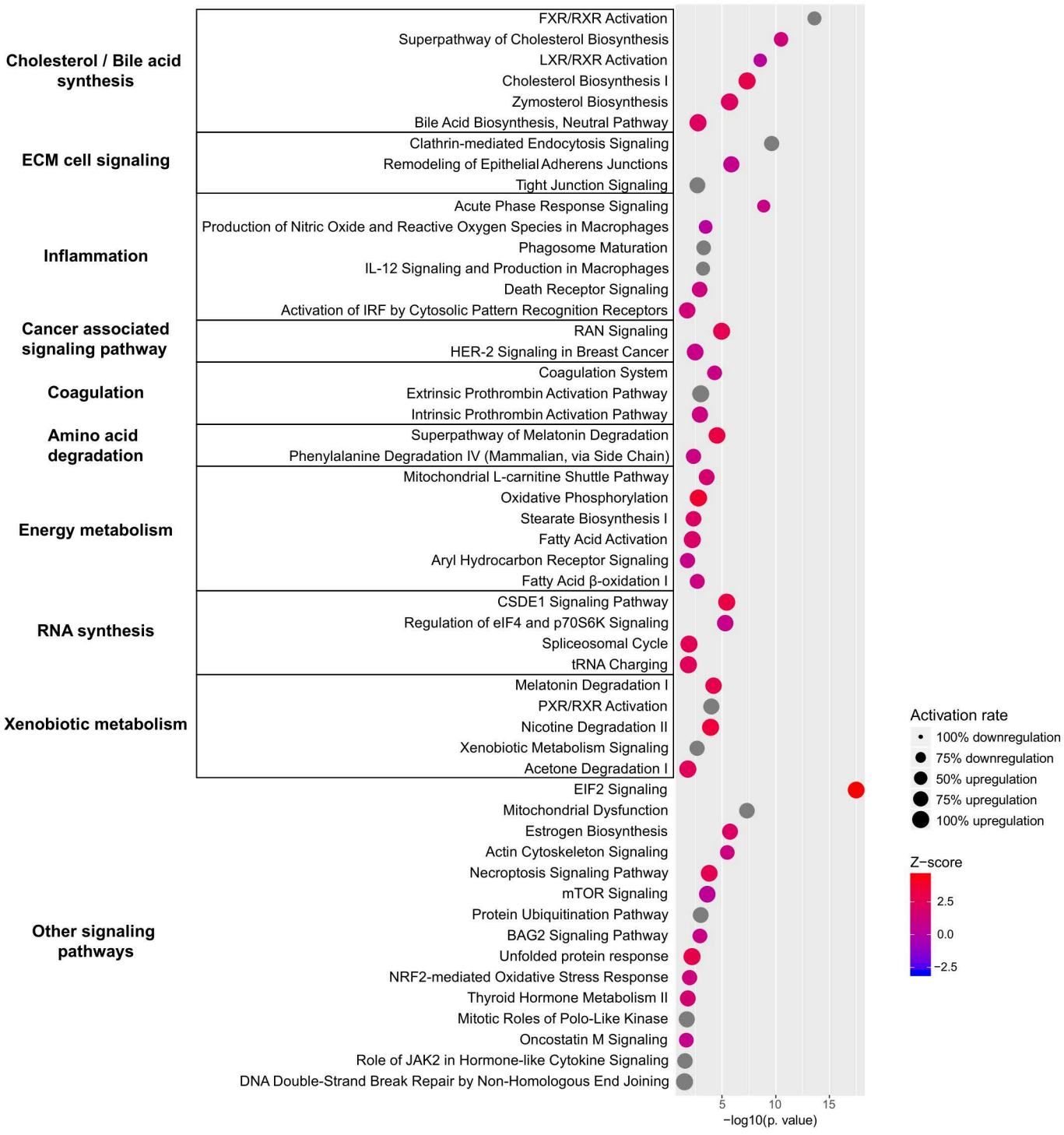

Supplementary Figure 6

F

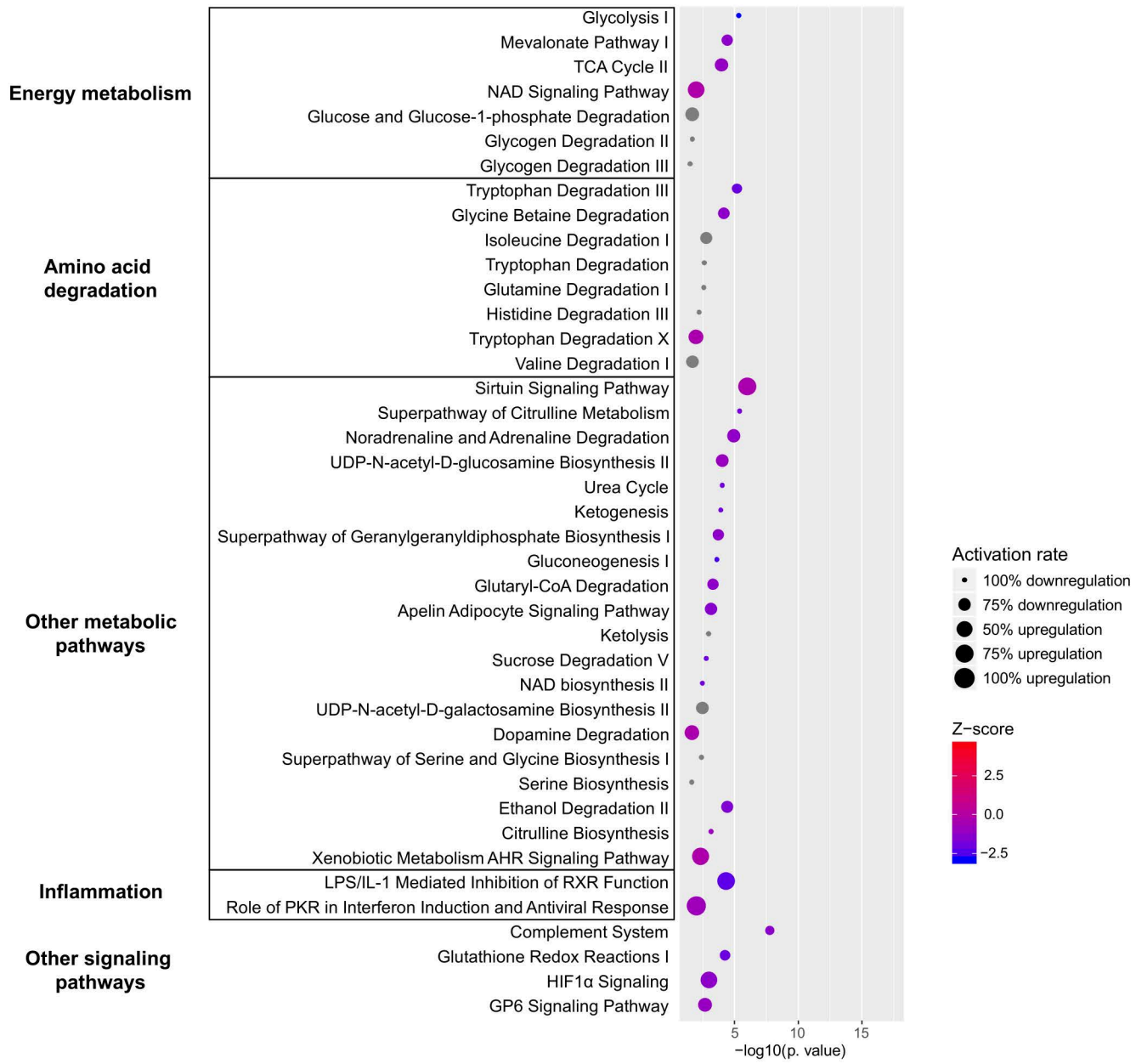

Supplementary Figure 6

G

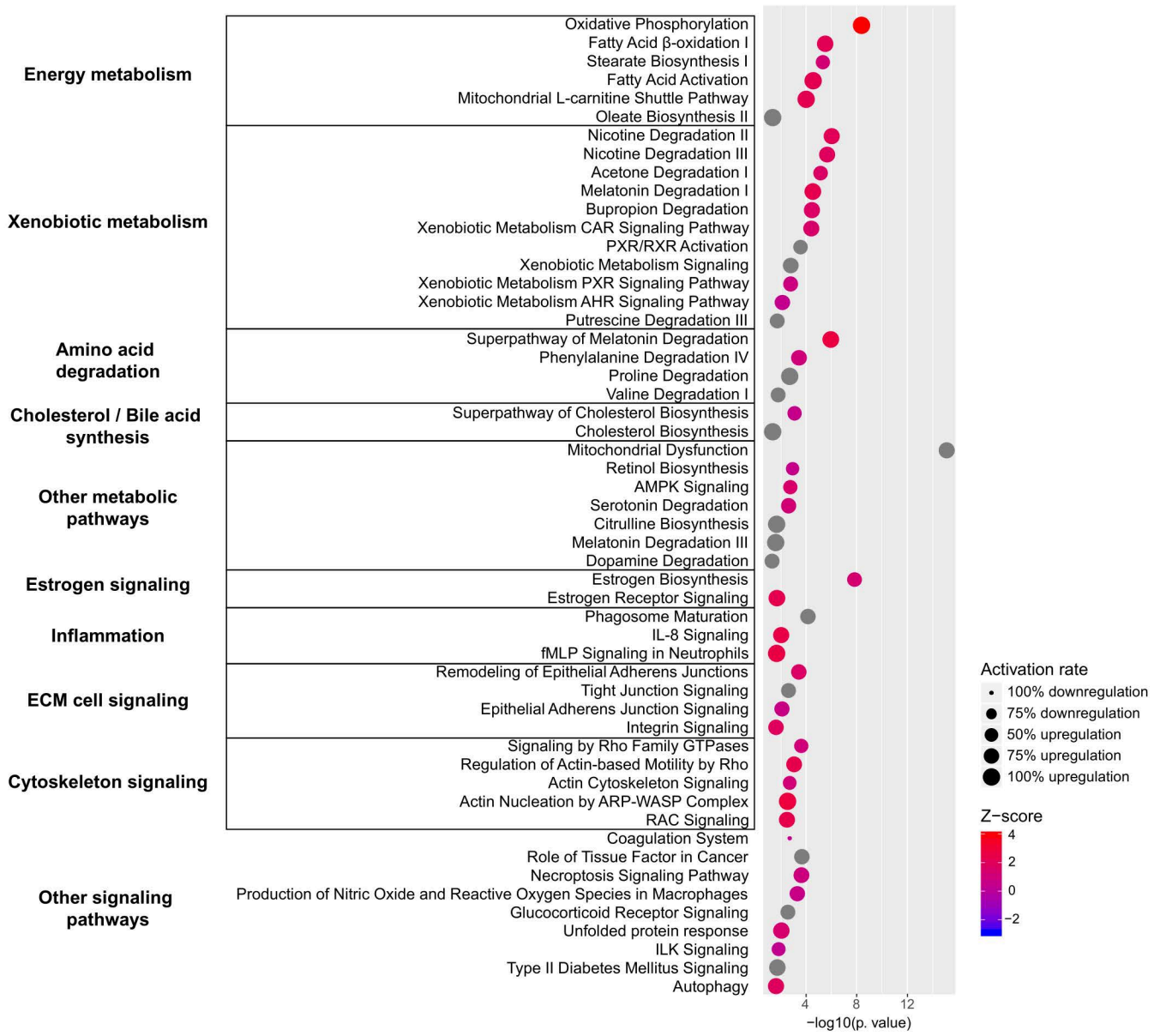

Supplementary Figure 6

H